Global Biogeochemical Cycles

RESEARCH ARTICLE
10.1029/2020GB006759

Key Points:

- The main characteristics and drivers of Deep Chlorophyll Maxima (DCM) are analyzed from a global BGC-Argo database
- Latitude and season determine the occurrence and characteristics of DCMs
- DCMs result from photoacclimation or biomass accumulation, depending on the availability of light and nitrate

Supporting Information:

Supporting Information may be found in the online version of this article.

Correspondence to:

M. Cornec,
cornec@obs-vlfr.fr

Citation:

Cornec, M., Claustre, H., Mignot, A., Guidi, L., Lacour, L., Poteau, A., et al. (2021). Deep chlorophyll maxima in the global ocean: Occurrences, drivers and characteristics. *Global Biogeochemical Cycles*, *35*, e2020GB006759. https://doi.org/10.1029/2020GB006759

Received 22 JUL 2020
Accepted 9 MAR 2021

Deep Chlorophyll Maxima in the Global Ocean: Occurrences, Drivers and Characteristics

M. Cornec[1], H. Claustre[1], A. Mignot[2], L. Guidi[1], L. Lacour[3], A. Poteau[1], F. D'Ortenzio[1], B. Gentili[1], and C. Schmechtig[1]

[1]CNRS & Sorbonne Université, Laboratoire d'Océanographie de Villefranche, LOV, Villefranche-sur-Mer, France, [2]Mercator Océan International, Ramonville-Saint-Agne, France, [3]Takuvik Joint International Laboratory, Laval University (Canada) - CNRS (France), Département de biologie et Québec-Océan, Université de Laval, Québec, QC, Canada

Abstract Stratified oceanic systems are characterized by the presence of a so-called Deep Chlorophyll a Maximum (DCM) not detectable by ocean color satellites. A DCM can either be a phytoplankton (carbon) biomass maximum (Deep Biomass Maximum, DBM), or the consequence of photoacclimation processes (Deep photoAcclimation Maximum, DAM) resulting in the increase of chlorophyll a per phytoplankton carbon. Even though these DCM (further qualified as either DBMs or DAMs) have long been studied, no global-scale assessment has yet been undertaken and large knowledge gaps still remain in relation to the environmental drivers responsible for their formation and maintenance. In order to investigate their spatial and temporal variability in the open ocean, we use a global data set acquired by more than 500 Biogeochemical-Argo floats given that DCMs can be detected from the comparative vertical distribution of chlorophyll a concentrations and particulate backscattering coefficients. Our findings show that the seasonal dynamics of the DCMs are clearly region-dependent. High-latitude environments are characterized by a low occurrence of intense DBMs, restricted to summer. Meanwhile, oligotrophic regions host permanent DAMs, occasionally replaced by DBMs in summer, while subequatorial waters are characterized by permanent DBMs benefiting from favorable conditions in terms of both light and nutrients. Overall, the appearance and depth of DCMs are primarily driven by light attenuation in the upper layer. Our present assessment of DCM occurrence and of environmental conditions prevailing in their development lay the basis for a better understanding and quantification of their role in carbon budgets (primary production and export).

1. Introduction

Our understanding of phytoplankton dynamics and their contribution to both photosynthetic carbon fixation and the biological carbon pump have largely benefitted from the improvement and the increasing availability of satellite observations of chlorophyll *a* concentration [Chl*a*], a proxy for phytoplankton biomass. Remote-sensing measurements are however restricted to a superficial layer (the so-called "first optical depth," Gordon & McCluney, 1975), whose thickness in the open ocean essentially depends on phytoplankton biomass and hence on [Chla] (Morel, 1988). Indeed, below this layer, Deep Chlorophyll Maxima (DCM), revealed by *in situ* observations, sometimes attest to the existence of potentially active phytoplankton communities at subsurface depths, obviously escaping satellite detection.

DCMs (sometimes also referred to as Subsurface Chlorophyll Maxima, SCM) express a pronounced peak in the vertical profiles of [Chl*a*]. DCM development requires stratified conditions (Estrada et al., 1993) that allow the establishment of a two-layer system, nutrient-limited above, and light-limited below (Beckmann & Hense, 2007; Dugdale, 1967; Hodges & Rudnick, 2004; Voituriez & Herbland, 1979). The interface between the two layers generally sets the environmental conditions favorable for the DCM to develop and occasionally be maintained (Beckmann & Hense, 2007; Cullen, 1982, 2015; Cullen & Eppley, 1981; Riley et al., 1949; Steele & Yentsch, 1960; Venrick et al., 1973). DCMs have been extensively studied since the 1970s (see Ardyna et al., 2013; Baldry et al., 2020; Cullen, 2015; Scofield et al., 2020 for recent and/or synoptic assessments, respectively, in the Arctic Ocean, using a global approach, in the North American lakes, and in the Southern Ocean). What primarily emerges from this abundant literature is that DCM features cover a wide range in term of characteristics (depth, magnitude, shape, Cullen, 1982; Hense & Beckmann, 2008; Lavigne

et al., 2015; Uitz et al., 2006), prevailing phytoplankton community and dominant physiological processes. Second, a number of different factors (both environmental and biological) may be involved in the formation (and endurance) of DCMs. In this way, the DCM is "*not a unique ecological response to environmental conditions; rather, a broad range of interacting processes can and generally do contribute to the formation of persistent subsurface layers of elevated Chl*" (Cullen, 2015).

All studies conducted so far have essentially focused on specific regions or seasons, using different methods for identifying and appraising their occurrence. As a consequence, while an overall picture has begun to emerge with respect to various types of DCMs and their potential drivers, their observation and characterization still remain too scarce and incomplete for the development of any possible generalizations. Furthermore, these observational gaps translate directly into knowledge gaps and potentially great uncertainties regarding the role of DCMs and their impact on carbon fluxes (e.g., primary production and carbon export, Morel & Berthon, 1989; Joint & Groom, 2000; Platt et al., 1988) at a global scale. Indeed, most estimations of primary production associated with DCMs are either localized, restricted to a specific area, or else based on modeling approaches (e.g., Ardyna et al., 2013; Pérez et al., 2006; Silsbe & Malkin, 2016). In this context, it appears essential to develop more global and comprehensive DCM observations, for advancing understanding on not only the establishment and functioning of DCMs, but also their role in carbon fluxes.

On the basis of our present understanding on DCMs, the intensification of observations should address two main objectives. The first objective relates to the prevailing environmental conditions associated with the establishment, maintenance and disappearance of DCMs. Stratified conditions (either permanent or transitory) are a prerequisite to DCM establishment. Stratification controls the flux of nutrients from below and the thickness of the mixed layer where these nutrients will eventually become available for phytoplankton growth (Huisman et al., 2006; Karl et al., 1995; Sharples et al., 2001). Meanwhile, surface irradiance together with the thickness of the mixed layer and its phytoplankton content control the flux of photons to the depth horizon where they may eventually encounter favorable nutrient conditions for phytoplankton growth and DCM formation (Banse, 1987; Hense & Beckmann, 2008; Letelier et al., 2004; Mignot et al., 2014; Taylor et al., 1986; Kemp et al., 2000). It follows that an ideally comprehensive data set for appraising environmental control of DCMs should encompass, together with the vertical distribution of [Chl*a*] and stratification conditions, key measurements of the two principal drivers of phytoplankton growth, namely light and nutrients (Cullen, 2015).

The second objective is related to the nature of the DCM: does it reflect a true increase in biomass in terms of phytoplankton carbon (Anderson, 1969; Barbieux et al., 2019; Beckmann & Hense, 2007; Herbland & Voituriez, 1977; Hodges & Rudnick, 2004; Holm-Hansen & Hewes, 2004; Kemp et al., 2000; Martin et al., 2010; Steele, 1964; Voituriez & Herbland, 1979), or is it solely a photoacclimation response to vanishing irradiance, unrelated to any cellular carbon increase (Fennel & Boss, 2003; Kiefer et al., 1976; Letelier et al., 2004; Mignot et al., 2014; Steele & Yentsch, 1960; Taylor et al., 1997)? Addressing this question represents a crucial step toward pinpointing the potential contribution and impact of DCMs on carbon fluxes. True biomass maxima, expected to result from additional production at the DCM level favored by more optimal light and nutrient conditions (Herbland & Voituriez, 1979; Kemp et al., 2000; Klausmeier & Litchman, 2001; Letelier et al., 2004), will probably have stronger influence on both primary production and carbon fluxes, than purely photoacclimation-driven DCMs (Maranon et al., 2000; Pérez et al., 2006; Westberry et al., 2008). Obviously, the actual answer is likely to be more nuanced and to fall between these two recognized endpoints of DCM characteristics (Cullen, 2015). Therefore, and in order to better assess DCM contributions to biomass on a global scale, observations would ideally combine [Chl*a*] measurements with concurrent estimations of Particulate Organic Carbon (POC) concentrations.

The development of new oceanic observing systems, along with the miniaturization of sensors, has led to the spread of autonomous platforms in the world ocean (Chai et al., 2020). The global network of Biogeochemical Argo (BGC-Argo) floats, having accumulated more than 10 years of pilot surveys in a variety of open-ocean areas, now provides a unique data set of vertical profiles with high spatial- and temporal-resolution measurements of physical and biogeochemical parameters (Claustre et al., 2020; Roemmich et al., 2019). Besides Temperature and Salinity, these measurements include vertical profiles of chlorophyll *a* fluorescence, a proxy for [Chl*a*] (Roesler et al., 2017), and of particle backscattering coefficients (b_{bp}), a proxy for POC (Cetinić et al., 2012; Loisel & Morel, 1998; Stramski et al., 1999). These measurements have

the potential to discriminate between DCMs corresponding to the effective accumulation of biomass (DBM: Deep Biomass Maxima) and DCM resulting from photoacclimation (DAM: Deep photoAcclimation Maxima). In addition to these measurements, BGC-Argo floats also carry irradiance and nitrate sensors, thus offering the potential to investigate the role of these key drivers of phytoplankton growth in controlling DCM establishment and characteristics.

In the present study, we use data from 505 profiling floats (75,473 profiles) deployed from 2010 to 2019 to develop a comprehensive inventory of DCMs in the world ocean. To our best knowledge, no such global assessment of DCMs using *in situ* data and homogeneous sampling has been proposed to date. Indeed, the many existing studies on, or referring to DCMs, are based on either sparse *in situ* measurements (ship-based, few BGC-Argo floats, glider transects; often limited in season and/or focused on a specific area), or modeling approaches. The strength of the present data set to address DCM typology and drivers not only resides in the embedded sensors performing high-resolution measurements, but also in the wide range of oceanic conditions explored, including various regions of the global open ocean with different trophic and hydrodynamic status, and over several annual cycles.

Overall, the goal of this study is to develop a stepwise analysis of the BGC-Argo data set in order to establish the bases of a possible generalization of DCM characteristics and of the conditions prevailing in their establishment and maintenance. More specifically, we aim at developing better understanding on their occurrence in space (regionally, vertically) and time (seasonally), their typologies (DAM vs. DBM) and their drivers (nutrients vs. light). In this context, our approach is organized as follows. We first use the BGC Argo data set to develop and apply a unique method for the detection of any DCM, and for its further classification into DBM or DAM. The distribution of DBMs and DAMs is then analyzed at various spatial and temporal scales together with specific metrics of DCM characteristics. Some of these metrics are further used to propose a classification of DCMs in the global ocean according to a few representative DCM types that obey singular patterns. Finally, we address the environmental parameters (nitrate and light fields, trophic environment, mixed layer dynamic) that prevail in the formation and maintenance of DCMs and ultimately control the global balance between DBMs and DAMs. (Note that the different acronyms and variables used in this study and their associated symbols, definitions, and units are detailed in Table 1).

2. Materials and Methods

2.1. The Initial Data set and Its Zonation

The present data set relies on 505 floats that have been deployed since 2010 in various regions of the global ocean in the context of different research programs. Besides CTD sensors, these floats are equipped with up to six additional sensors measuring the core BGC-Argo variables (Claustre et al., 2020; Roemmich et al., 2019), namely [Chl*a*], b_{bp}, PAR, oxygen, nitrate and pH. As of December 31, 2019, a total of 75 473 [Chl*a*] and b_{bp} vertical profiles had been collected, the core data set used in the present analysis (Figure 1, Argo, 2020). To describe the environmental context of the vertical profiles of [Chl*a*] and b_{bp}, we additionally use, when present, vertical profiles of PAR, nitrate and oxygen. Most of the floats included are official BGC-Argo floats and accessible through the Coriolis database (ftp://ftp.ifremer.fr/ifremer/argo). Some other float data were derived from 13 floats in the North Atlantic (http://misclab.umeoce.maine.edu/floats/), and 3 floats in the South China Sea (Haili Wang, pers. comm.).

From the global data set, 7 094 profiles (9.4% of global database profiles) were removed, either because they were insufficiently representative of a given area (too few data to allow further analysis), or potentially influenced by coastal waters (using bathymetry data from the General Bathymetric Charts of the Ocean (GEBCO_2020), profiles matching a bathymetry shallower than 1,500 m were discarded), or not representative enough of a given area because of local effects (e.g., the Marquesas Islands area, in the central Pacific, whose subequatorial waters are biased by recurrent blooms in their vicinity).

2.2. Qualification of Physical Profiles and Derived Quantities

Following Argo protocols, hydrological data collected by the SBE 41 Seabird CTD sensors were processed and quality-controlled as described by Wong et al. (2020). The Mixed Layer Depth (MLD) was calculated

Table 1
Acronyms, Definitions and Units

Symbol	Definition	Unit
BGC	Biogeochemical	
CTD	Conductivity Temperature Density	
DAM	Deep photoAcclimation Maximum	
DBM	Deep Biomass Maximum	
DCM	Deep Chlorophyll Maximum	
MAE	Mean Absolute Error	
R^2.adj	Adjusted correlation coefficient	
RMSE	Root Mean Square Error	
POC	Particulate Organic Carbon	mg C m^{-3}
b_{bp}	particulate backscattering coefficient	m^{-1}
[Chl*a*]	Chlorophyll *a* concentration	mg chl*a* m^{-3}
$[Chla]_{sat}$	Chlorophyll *a* concentration measured from satellite	mg chl*a* m^{-3}
iPAR	Daily integrated PAR	E m^{-2} d^{-1}
$iPAR_{20}$	Isocline of iPAR of 20 E m^{-2} d^{-1}	m
$iPAR_{Nit}$	iPAR at the nitracline depth	E m^{-2} d^{-1}
$\overline{iPAR}_{ML}$	Mean iPAR in the Mixed Layer	E m^{-2} d^{-1}
K_d	PAR diffuse attenuation coefficient	m^{-1}
ML	Mixed Layer	
MLD	Mixed Layer Depth	m
m_{Nit}	Nitracline steepness	µmol NO3 m^{-3} m^{-1}
N2	Brunt-Vaisala frequency	Hz
$N2_{Nit}$	Brunt-Vaisala frequency at the nitracline depth	Hz
$\overline{Nitrate}_{ML}$	Mean Nitrate concentration in the Mixed Layer	µmol NO3 m^{-3}
PAR	Photosynthetically Available Radiation	E m^{-2}
q_{25}	25th percentile	
q_{75}	75th percentile	
TSWS	Typical Stable Water Structure	
Z_{nit}	Nitracline depth	m
Z_{pd}	First Optical Depth	m

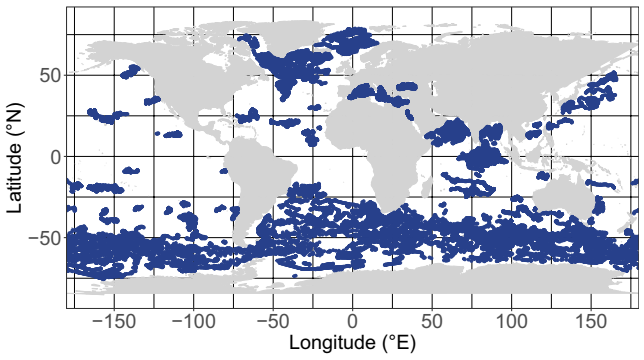

Figure 1. Map of the BGC-Argo profiles where the [Chl*a*] and the b_{bp} are measured. BGC, Biogeochemical.

using the density differential threshold criterion of 0.03 kg m^{-3} with reference to the density at 10 m (de Boyer Montégut et al., 2004). This criterion is considered as the most appropriate for a global-scale approach. To obtain an estimation of the stratification strength along the vertical profile, the square of the Brunt–Väisälä frequency or buoyancy frequency (N2) was also calculated for each profile depth from the temperature and salinity values.

2.3. Qualification of [Chl*a*] and b_{bp} Profiles

The floats were equipped with Seabird-Wetlabs sensors of three types (FLBB, ECO-Triplet, or MCOMS). All sensor types included a Chl*a* fluorometer (excitation at 470 nm; emission at 695 nm), and a backscattering sensor at 700 nm. To establish an interoperable and homogeneous data

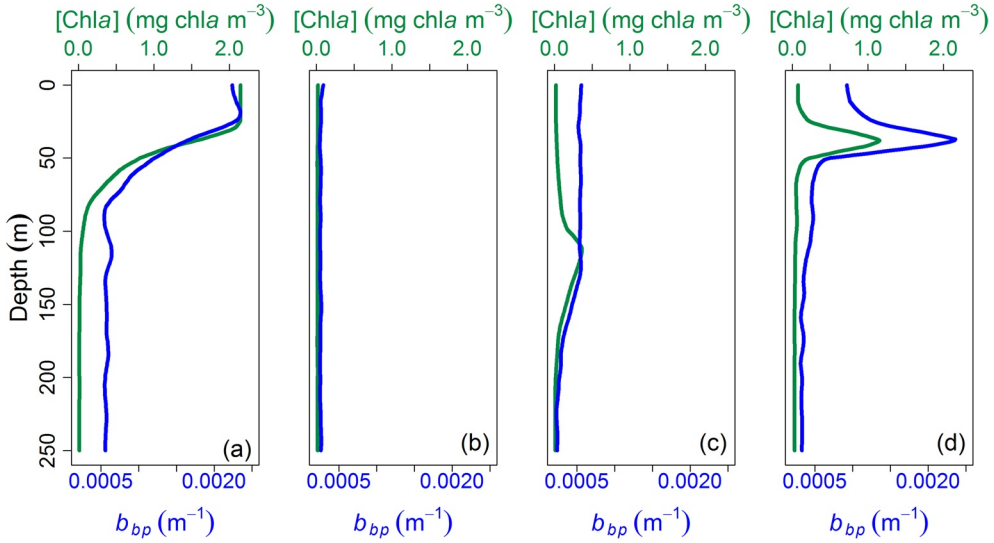

Figure 2. Example of vertical profiles of [Chl*a*] (green) and b_{bp} (blue) classified as (a), (b) NO, (c) DAM, and (d) DBM. DAM, Deep photoAcclimation Maximum; DBM, Deep Biomass Maximum.

set regardless of the specific procedures used by different Argo Data Centers (not at the same level of maturity at the time of the present analysis), all vertical profiles of [Chl*a*] fluorescence and b_{bp} were processed from raw data (numerical counts). The procedures are described in detail by Bellacicco et al. (2019) and include: conversion of numerical counts into [Chl*a*] and b_{bp} physical units; visual quality control of the profiles and potential sensor-drift corrections; removal of out-of-range values; dark-offset correction for the [Chl*a*]; correction for non-photochemical quenching for the [Chl*a*]. A factor-two correction was applied to account for [Chl*a*] overestimation by Seabird-Wetlabs fluorometers (Roesler et al., 2017). Similarly, b_{bp} processing took into account new calibration factors provided by Seabird-Wetlabs, following inconsistencies identified among various types of b_{bp} sensors (Poteau et al., 2017). Altogether, following this careful data screening and correction, 56 624 profiles (i.e. 75% of the global database profiles) were finally kept for the present analysis.

2.4. Identification and Classification of Deep Maxima Profiles

An algorithm detailed below allowed the shape of the [Chl*a*] and b_{bp} profiles to be classified when any Deep Chlorophyll Maxima were detected. Basically, three profile types were defined (Figure 2): (1) NO deep maxima, corresponding to either mixed waters or near-surface [Chl*a*] and b_{bp} maxima generally associated with blooms; (2) DAM (Deep photoAcclimation Maximum) types, corresponding to a [Chl*a*] maximum not reflected in a b_{bp} maximum and essentially resulting from phytoplankton photoacclimation to low irradiance; (3) DBM (Deep Biomass Maximum) types, presenting maxima in both b_{bp} and [Chl*a*] and corresponding to a true increase in phytoplankton biomass (e.g., in terms of carbon). In the following, DAM and DBM will be referred to collectively as DCM (Deep Chlorophyll Maxima).

Most profiles (38 273, 51% of the global database profiles) of [Chl*a*] and b_{bp} present a high vertical resolution (an average vertical resolution above 3 m in the top 250 m). With an approximative constant prevalence for spikes, higher resolution data gives a higher chance of a spike occurence, which is not our present interest. Therefore, [Chl*a*] and b_{bp} profiles were first smoothed (a 5-point running median filter for [Chl*a*]; a 5-point running median filter followed by a 5-point running mean filter for b_{bp}) to allow the retrieval of the profile shape free from spikes and background noise. For coarser resolution profiles (>3 m in the top 250 m, 26 059 profiles, 35% of the global database profiles) no smoothing was applied on both [Chl*a*] and b_{bp}. Both methods give compatible results when delineating at 3 m average resolution (see supportive information, Text S1 and Figures S1–S5). All profiles were then identically treated for the next steps.

The depth of the [Chl*a*] maximum was then searched for between 0 and 300 m, assuming that no phytoplankton [Chl*a*] can develop below 300 m (note that [Chl*a*] maxima can be identified below 300 m but they result from advective transport due to eddy subduction, e.g., see Llort et al., 2018). Once the maximum and depth were identified on the smoothed profile, the closest [Chl*a*] measurements on the unsmoothed profile were accordingly identified. The profile was definitively qualified as a DCM if the maximum [Chl*a*] value of the unsmoothed profile was greater than twice the median of the [Chl*a*] values in the 15 first meters (Lavigne et al., 2015). Otherwise, it was qualified as NO.

The potential cooccurrence of the DCM depth with any deep peak of b_{bp} was subsequently tested. The depth of the b_{bp} maximum was searched for from the smoothed b_{bp} profile in a layer of 20 meters around the DCM depth. As for the [Chl*a*] profile, once the b_{bp} maximum and depth were identified on the smoothed profile, the closest b_{bp} measurements on the unsmoothed profile were accordingly identified. The profile was defined as a DBM if the b_{bp} maximum was more than 1.3 times the b_{bp} minimum within the top 15 meters. Otherwise, it was qualified as a DAM, that is, where the [Chl*a*] maximum did not match a b_{bp} maximum. The choice of this criterion was derived from the analysis of DBM signature along vertical BGC-Argo profiles of optical proxies (including b_{bp}) in oligotrophic regions by Mignot et al. (2014). The criterion was subsequently refined and tested on several profiles representative of our global data set.

2.5. PAR Attenuation Coefficient and Daily Integrated PAR

The irradiance prevailing at the depth of DCMs was assessed thanks to PAR sensors (OCR Sensor Seabird-SATLANTIC) equipping some of the floats (36,423 profiles, 48% of the global database profiles, supportive information, Figure S6). For floats without PAR sensors, PAR profiles were modeled. This was achieved by first retrieving surface PAR under cloud-free conditions using a clear-sky model (Gregg & Carder, 1990). This irradiance was further propagated along the vertical dimension thanks to a diffuse attenuation coefficient (K_d) derived from empirical bio-optical relationships (Morel, Huot, et al., 2007) which, here, were refined on the basis of similar groups of regions (see supportive information, Text S2 and Figure S7). Finally, in order to transform the clear-sky-modeled profile into a PAR profile corresponding to real, potentially cloudy conditions, we used the method of Lacour et al. (2017). This method derives a correction coefficient from the ratio of the *in situ* profile to the model-estimated PAR profile (mean cloud cover during the float ascent). We used the profiles with *in situ* PAR measurements and associated model-estimated PAR profiles to estimate cloud-cover correction coefficients per month and per band of 10° latitude. These coefficients (supportive information, Table S1) were then re-applied on the rest of the model-estimated PAR profiles (i.e., those floats without PAR sensors). The daily integrated PAR (iPAR) was calculated at each depth by integrating modeled PAR profiles over the day-length as described by Lacour et al. (2017). For each profile, the average daily iPAR in the mixed layer ($\overline{iPAR_{ML}}$) was calculated as the integral of iPAR values in the mixed layer divided by the MLD.

2.6. Nitrate, Nitracline Depth and Steepness of the Nitracline

While a number of BGC-Argo floats are not equipped with nitrate sensors, nearly all of them do have oxygen ones. From oxygen and hydrological profiles together with float geolocation, the nitrate profiles were estimated using the so-called CANYON B neural network (Bittig et al., 2018; Sauzède et al., 2017), which presents an accuracy of 0.68 μmol kg^{-3} for the retrieval of nitrate concentrations, and an uncertainty of 0.99 of μmol kg^{-3} (Bittig et al., 2018).

The nitracline depth (Z_{nit}) and steepness (m_{Nit}) were subsequently estimated for each profile as proxies for better characterization of the DCMs' nutrient environmental context. Several methods for each metric (i.e., Z_{Nit} and m_{Nit}) were initially tested on a subset of profiles representative of oceanic-region diversity in the database (supportive information, Text S3 and Figures S8 and S9). Finally, the nitracline depth was defined as the depth at which exists a concentration difference of 1 μmol L^{-1} with reference to the surface value, adapted from Lavigne et al. (2015). Meanwhile, the steepness of the nitracline (m_{Nit}) was defined as the slope of the linear regression of nitrate values as a function of depth in a layer between the nitracline depth and 1.25 times the nitracline depth.

Both nitrate-related metrics Z_{nit} and m_{Nit} and their calculation methods are robust with respect to any possible deviations of the nitrate concentration (derived from the CANYON B neural network) because they are based on the shape of the nitrate profile rather than on the absolute concentrations themselves. Note that m_{Nit} is significantly related to the Brunt–Väisälä frequency (N2) at the nitracline depth (supportive information, Figure S10).

2.7. Matching Satellite [Chl*a*] and BGC-Argo Profiles

Surface [Chl*a*] measured by satellite ($[Chla]_{sat}$) can be considered as a metric on the trophic status prevailing at a given oceanic location (e.g. from oligotrophic conditions of the South Pacific Subtropical Gyre to the eutrophic conditions associated with the spring bloom in the North Atlantic Subpolar Gyre). The trophic gradient is defined as in Antoine et al. (1996): oligotrophic waters corresponds to a $[Chla]_{sat}$ below 0.1 mg chl*a* m^{-3}; mesotrophic are defined for a $[Chla]_{sat}$ range from 0.1 to 1 mg chl*a* m^{-3}; and eutrophic waters for $[Chla]_{sat}$ above 1 mg chl*a* m^{-3}. Independently from the [Chl*a*] measured by floats, $[Chla]_{sat}$ therefore provides a potentially useful way to upscale findings from the BGC-Argo database to the global ocean. Taking the $[Chla]_{sat}$ as reference instead of float surface [Chla] to establish such trophic status discards any uncertainties linked to the Fchl*a* retrieval from of BGC-Argo floats due to regional variability (Roesler et al., 2017), and potentially due to the variability in the NPQ correction (e.g. Xing et al., 2018). In this context, each BGC-Argo profile was matched with a L3S [Chl*a*] product from the Ocean Color-Climate Change Initiative v4.0 database merging observations from MERIS, MODIS, VIIRS and SeaWiFs, at a monthly and 4 × 4-km-pixel resolution, up to December 31, 2019 (ftp://oc-cci-data:ELaiWai8ae@oceancolour.org/occci-v4.2/).

2.8. Clustering Method for the Classification of Regions

In order to reveal robust patterns of DCM features in the various regions of the global ocean, profiles were divided into 28 regions a priori presenting coherent hydrological and/or biogeochemical patterns (supportive information: Text S4, Figure S11, and Tables S2–S4). We grouped these regions according to their mean properties with respect to four metrics: mean DCM depth, mean [Chl*a*] at the DCM depth, annual occurrence of DCM profiles, and annual occurrence of DBM profiles. The groups of regions were objectively defined using a K-means clustering method. *A priori* 2 to 10 groups were tested, with a maximum of 10 iterations, using the Hartigan & Wong algorithm (supportive information, Figure S12).

In this study, spring, summer, autumn and winter seasons, respectively, correspond to the months 3–5, 6–8, 9–11, and 12, 1, 2. Note that to develop informative representation of seasonal trends in both hemispheres, Southern Hemisphere data were shifted by 6 months with respect to Northern Hemisphere data.

2.9. Analytical and Statistical Methods, Softwares

To statistically compare mean region/group properties, the normality of the samples was tested (the Shapiro-Wilk test if the sample size was below 50; the Kolmogorov-Smirnov test, if greater than 50). If samples were normal, the significance of any difference was tested using the Welch test. When data were not normally distributed, the Mann-Whitney Wilcoxon test was used instead.

All data were treated and analyzed using R and Rstudio softwares (versions 3.2.3 and 1.1.3, respectively).

3. Results

3.1. General Deep Chlorophyll Maxima Characteristics

3.1.1. Latitudinal and Seasonal Occurrence of Deep Chlorophyll Maxima

To address the regional and seasonal variabilities of DCMs in the global ocean, the mean of the monthly percentages of DCM, DAM and DBM profiles, out of the total profile number, were aggregated over 10°-latitude bands (values calculated on ±5° range, centered on the tens) (Figure 3). The resulting global distribution of the DCMs presents a dome-like shape, nearly symmetrical, on either side of the Equator. The occurrence of

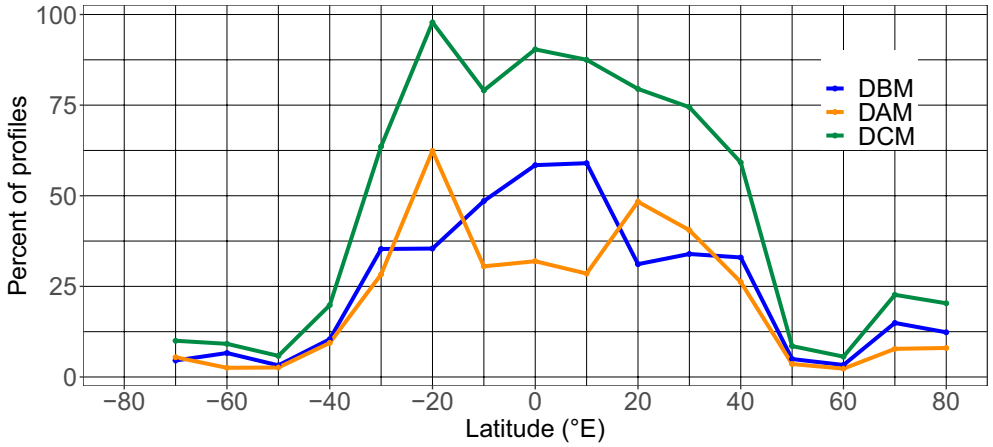

Figure 3. Mean of monthly percentage of profiles with DCM (green), DBM (blue), and DAM (orange) characteristics as a function of the latitude (per band of 10°). The percentage of DCMs corresponds to the sum of the percentages of DAMs and DBMs. DAM, Deep photoAcclimation Maximum; DBM, Deep Biomass Maximum; DCM, Deep Chlorophyll Maximum.

DCMs is greater than 50% at low latitudes (from 30°S to 40°N), with values over 75% from 20°S to 20°N. This occurrence decreases significantly toward high latitudes (below 25% above 40°), with a slight recrudescence recorded around 70°N (23%). DCMs therefore appear to be a dominant feature in equatorial, subequatorial (from 0 to ∼15°) and subtropical waters (from 15 to ∼35°).

In equatorial and subequatorial waters (0–10°), DCMs are dominated by DBMs (reaching 65% of total profiles at the Equator). Conversely, in subtropical waters (20°), DCMs are dominated by DAMs. The contributions of DAMs and DBMs to the total DCM profiles are then proportionally equivalent from 30° to the high latitudes (despite a higher proportion of DBMs at 70°N).

To address the seasonal variability of DCMs and of their two types, DAM and DBM, as a function of latitude, the 10°-aggregated profiles were subsequently analyzed at a monthly scale (Figure 4). From 0 to 20°, the proportion of DCMs remains stable throughout the year (close to or higher than 75% for each month). Strong seasonality appears at 30°: from May to October (recalling here that Southern Hemisphere data were shifted by 6 months), DCMs are found in almost 100% of the profiles; November and April are transition months with 75% having DCM profiles while only 50% of DCMs subsist in December and less than 25% in the remaining months. This seasonal pattern is also observed at 40°, but with a smaller magnitude. From 50 to 70°, the period of DCM occurrence narrows to the summer months (7 and 8), and stays below 10% the rest of the time.

As for the distribution of DBMs and DAMs, from 0 to 10°, the proportion of DBMs and DAMs is stable nearly all year long (∼50% for DBMs and ∼25% for DAMs). At 20°, DBMs present more seasonality: less than 25% from November to February, more than 40% from April to June, and around 35% from July to October. Meanwhile, DAMs are stable at around 50% from February to August, then exceed 60% from October to January. At 30°, DCMs are dominated by DBMs in spring and summer (>50% from May to July), and by DAMs in fall (>50% in October and November). At 40°, DBMs increase from virtually no presence in winter to up to 60% in August before decreasing again in autumn while DAM proportions show peaks during the spring and the autumn (exceeding 25% in May and October). From 40 to 60°, DBM and DAM proportions are equivalent (both below 2% from October to April, and reaching ∼10% in summer). At 70°, DBMs dominate DCMs, especially during summer (nearly 25% in August and September).

3.1.2. Latitudinal Distribution of Deep Chlorophyll Maxima Depth and Intensity

DCM depth and intensity (here estimated through [Chl*a*] and b_{bp} at DCM depth) present quasi-symmetric latitudinal distributions on either side of the Equator (Figures 5a and 5b). In equatorial and subequatorial waters (0–10°), DCMs are found at a mean depth of 61 m with a corresponding median [Chl*a*] of 0.58 mg chl*a* m^{-3}, and a median b_{bp} of 10 10^{-4} m^{-1}. As expected, the deepest and least intense DCMs

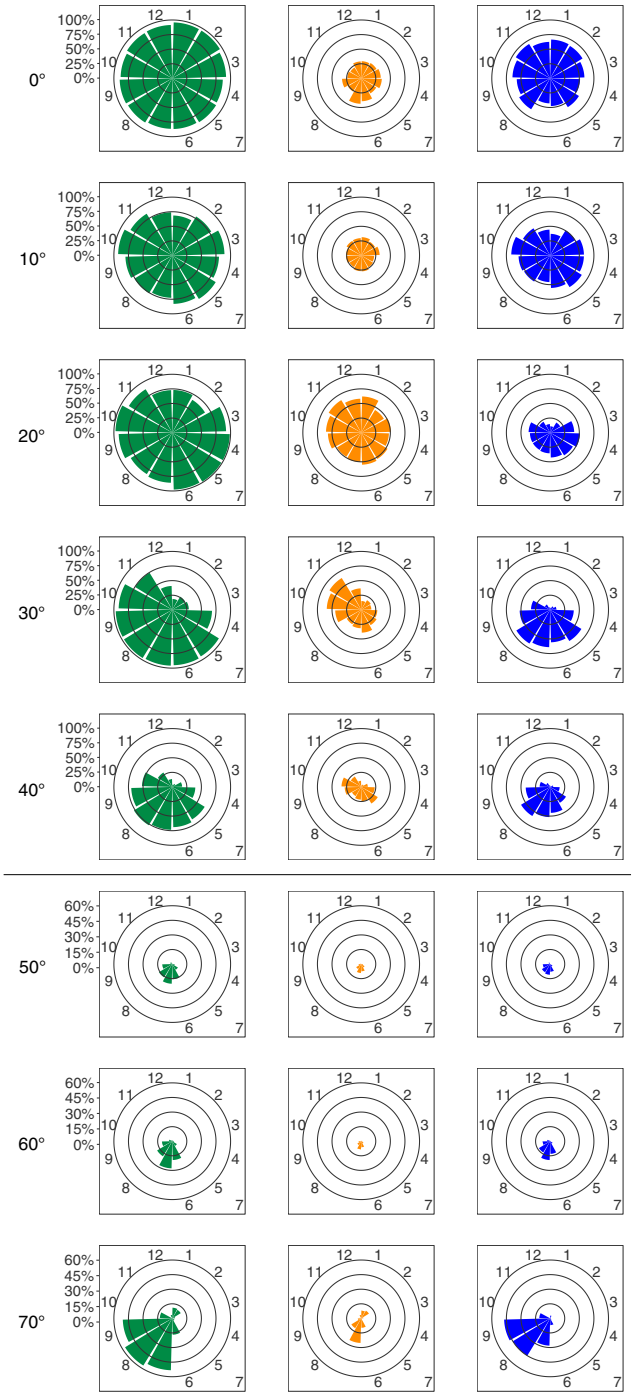

Figure 4. Percentage of profiles with DCM (green), DBM (blue), and DAM (orange) characteristics as a function of the absolute latitude (per band of 10°) and of the Northern Hemisphere-phased month (regardless of the year). Note the change in percentage scale between the 0–40° and 50–70° latitudinal bands. DAM, Deep photoAcclimation Maximum; DBM, Deep Biomass Maximum; DCM, Deep Chlorophyll Maximum.

are recorded in subtropical waters, with the most extreme characteristics found in the south (mean depth = 124 m; [Chl$a$] = 0.32, mg chl$a$ m^{-3}; b_{bp} = 6 10^{-4} m^{-1} at 20°S) rather than in the north (mean depth = 84 m; [Chl$a$] = 0.36 mg chl$a$ m^{-3}; b_{bp} = 7.4 10^{-4} m^{-1} at 20°N). The 30–50° latitudinal bands are transitional locations where DCMs rapidly shallow and become more intense (e.g., at 50°N: mean depth = 41; [Chl$a$] = 0.96 mg chl$a$ m^{-3}; b_{bp} = 20 10^{-4} m^{-1}; vs. at 50°S: mean depth = 64 m; [Chl$a$] = 1.00 mg chl$a$ m^{-3}; b_{bp} = 22 10^{-4} m^{-1}). At northern polar latitudes, DCMs are shallow and intense (e.g., at 70°N: mean depth = 39 m; [Chl$a$] = 1.63 mg chl$a$ m^{-3}; b_{bp} = 24 10^{-4}, m^{-1}). In contrast, at high latitudes of the Southern Hemisphere, DCMs are less shallow and intense (e.g., at 70°S: mean depth = 53 m; [Chl$a$] = 1.02 mg chl$a$ m^{-3}; b_{bp} = 16 10^{-4} m^{-1}). The dispersion of the mean or median parameters per 10°-latitudinal bands is provided in the supportive information: Table S5. At global scale, [Chl$a$] and b_{bp} at the DCM depth appear to covary at first order (supportive information: Text S6 and Figure S13). However, this covariation is weaker for DAM that for DBM profiles, which likely reflects either a shift in phytoplankton communities or the signature of photoacclimation process for DAMs with respect to DBMs. Addtionnally, DCM depth also appears to be negatively related to the trophic status in the upper layer of the water column, estimated by the [Chl$a$]$_{sat}$ (supportive information: Text S7 and Figure S14)

3.1.3. Daily Light Availability in the Mixed Layer: A Primary Indicator of Deep Maxima Presence

The mean daily PAR within the mixed layer ($\overline{iPAR}_{ML}$) is used to investigate the potential impact of light availability in the upper layer of a profile on the DCM occurrence at depth (Figure 6). This metric choice allows the comparison of profiles from different trophic regimes (i.e., with different Chl$a$ concentrations) and physical regimes (with different mixed layer (ML) thicknesses) to find out how these may drive light attenuation within the ML and its subsequent availability at DCM depth. Profiles with DCMs are characterized by higher $\overline{iPAR}_{ML}$ (median of 29.2, q_{25} = 17.57, q_{75} = 40.23 E m^{-2} d^{-1}) than profiles without maxima (median of 6.12, q_{25} = 2.45, q_{75} = 13.10 E m^{-2} d^{-1}). The two distributions are significantly different (Wilcoxon test, p-value < 2.2 10^{-16}). We note that the $\overline{iPAR}_{ML}$ at DCMs is not significantly different for the four clustered groups or regions (see next section; data not shown).

3.1.4. Region Clustering Based on Deep Maxima Properties

To further investigate the coherent spatial and seasonal patterns revealed in the above global observations, we chose to classify the 28 regions into four groups (K-Means clustering, supportive information, Figure S12). This classification was based on similarities in four DCMs properties: DCM depth, mean [Chl$a$] at the DCM depth, proportion of DCM and of DBM profiles (both implicitly encompassing the proportion of DAM profiles). The main DCM characteristics of each of these four groups are evidenced in Figure 7. The first group (orange, called Deep photoAcclimation Zones (DAZ)), is distinguished by having the weakest (median of 0.46 mg chl$a$ m^{-3}) and deepest (mean of 107 m) DCMs with the highest yearly occurrence (mean of 86%); it is essentially composed of DAMs (mean DBM occurrence of only 34%). The second group (blue, Deep Biomass Zones (DBZ)) also presents a high proportion of DCMs

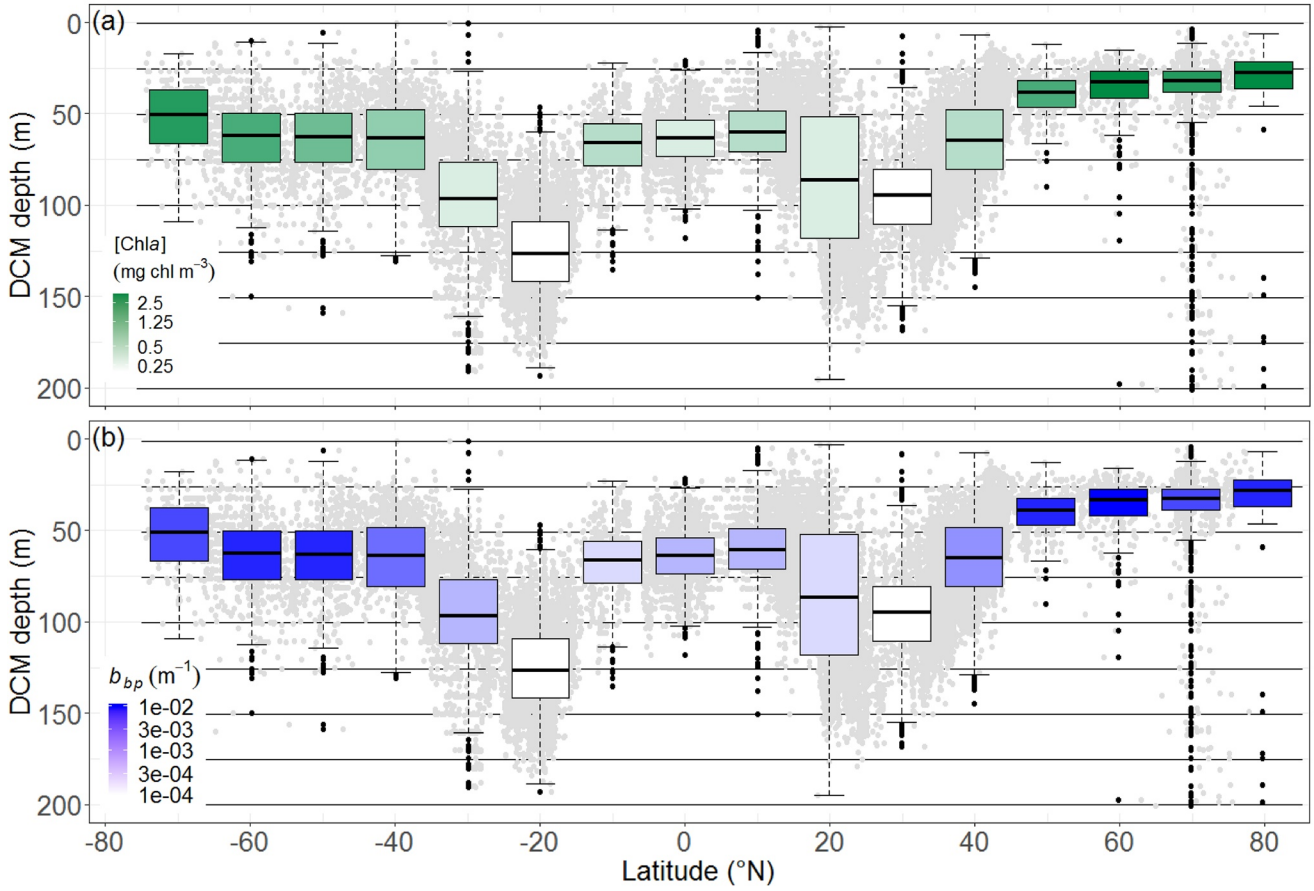

Figure 5. DCM depths (gray dots) and their quartile diagrams per 10° latitude. The mean [Chl*a*] and b_{bp} at the DCM depth are color-coded with a white-green log scale (a), and a white-blue log scale (b). DCM, Deep Chlorophyll Maximum.

(mean of 78%) occurring at shallower depths (mean of 57 m) with intermediate intensities (median of 0.78 mg chl*a* m^{-3}) and the highest proportion of DBM profiles (mean of 54%). The third group (brown, Ghost Zones (GHOZ)) exhibits the lowest occurrences of DCMs and DBMs (respectively means of 14% and 8%) with intermediate intensities (median of 1.28 mg chl*a* m^{-3}) and located at intermediate depths (mean of 64 m). The fourth group (purple, Shallow Maxima Zones (SHAZ)) also shows a low occurrence of DCMs and DBMs (means of 17% and 8%) which are shallow (mean of 37 m) and cover a wide spread of high intensities (median of 2.01 mg chl*a* m^{-3}). The dispersion of the four mean or median DCM properties for the four group of regions is described in the supportive information: Table S6.

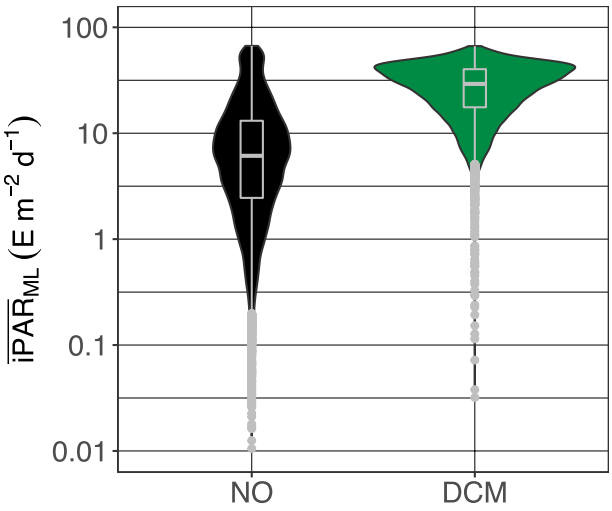

Figure 6. Quartile diagrams and density plots of the mean daily PAR in the mixed layer ($\overline{iPAR}_{ML}$) for DCM (green) and NO profiles (black). DCM, Deep Chlorophyll Maximum; PAR, Photosynthetically Available Radiation.

The resulting classification of the 28 regions into four groups with coherent DCM patterns follows, with only a few exceptions, a clear global latitudinal distribution (Figure 8). The SHAZ group encompasses most northern regions (the north subpolar gyres, the east Greenland waters, the Arctic Waters), and the Black Sea. The GHOZ group includes all the Southern Ocean waters (SubTropical Zone, Sub Antartic Zone, Polar Frontal Zone, and Antarctic Southern Zone/Seasonal Ice Zone) as well as the North Atlantic Current. The DAZ group includes most oligotrophic waters (the five subtropical gyres, the Archipelagos waters, the Eastern Basin of the Mediterranean Sea). The DBZ group includes most equatorial and subequatorial waters (i.e., from 0 to ~15°, Atlantic and

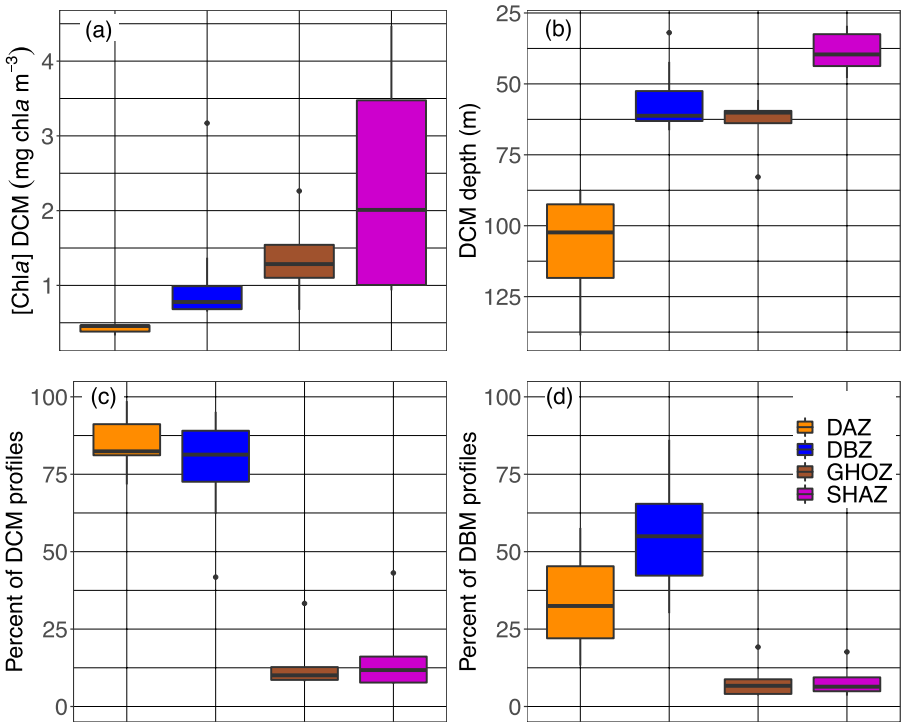

Figure 7. Quartile diagrams of DCM characteristics for the four groups (i.e., Shallow Maxima Zone, SHAZ; Ghost Zone, GOHZ; Deep photoAcclimation Zone, DAZ; and Deep Biomass Zone, DBZ) from the 28 clustered regions: (a) mean [Chl*a*] at DBM depths, (b) mean DBM depths, (c) mean percentage of DCM profiles, and (d) mean percentage of DBM profiles. DBM, Deep Biomass Maximum; DCM, Deep Chlorophyll Maximum.

Pacific SubEquatorial Waters, Indian Oxygen Minimum Zones, Indian Equatorial Waters, South Chinese Sea, Moonsoun Zone, and Western Australian Waters) as well as Baffin Bay, the Red Sea, and the Western Mediterranean Basin.

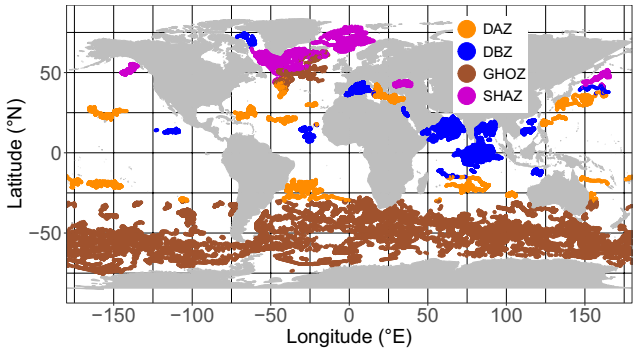

Figure 8. Spatial distribution of the global data set clustered into four groups (i.e., Shallow Maxima Zone, SHAZ; Ghost Zone, GOHZ; Deep photoAcclimation Zone, DAZ; and Deep Biomass Zone, DBZ) according to metrics relevant to DCM characteristics (mean DCM intensities, DCM depths, DCM and DBM occurrence). DCM, Deep Chlorophyll Maximum.

3.2. Environmental Conditions in the Four Typical Zones

On the basis of four metrics chosen to represent the characteristics of light and nutrient fields and their interactions in the vicinity of the DCM depth, we compared the environmental conditions at the DCM depth in the four zones (Figure 11): Shallow Maxima Zone (SHAZ), Ghost Zone (GOHZ), Deep photoAcclimation Zone (DAZ), and Deep Biomass Zone (DBZ). Note that the dispersion values of the different environmental parameters are described in the supportive information for the four zones (supportive information: Table S6).

3.2.1. Surface $[Chla]_{sat}$

The surface $[Chla]_{sat}$ (as described in Sections 2.7 and 3.1.2), gives an estimate of the trophic status prevailing in each zone (Figure 9a). It is the most intense for SHAZ (median of 0.53 mg chl*a* m^{-3}) followed by GHOZ and DBZ (respectively medians of 0.18 and 0.15 chl*a* m^{-3}), the latter two groups not being significantly different (Mann-Witney test, p-value of

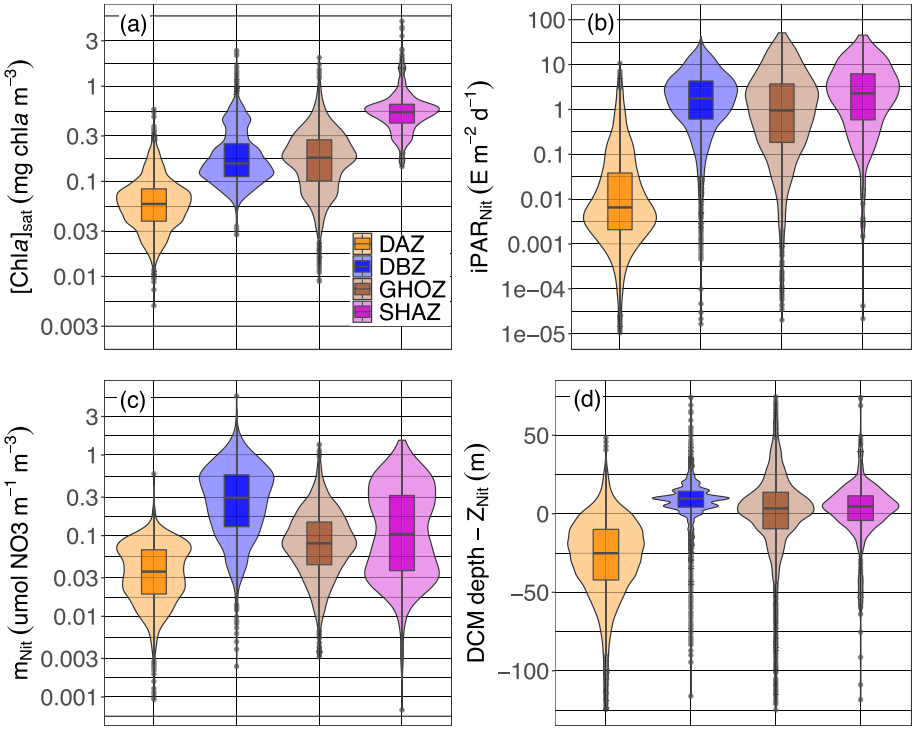

Figure 9. Quartile diagrams and density plots of the environmental characteristics of DCM profiles according to the four groups (i.e., Shallow Maxima Zone, SHAZ; Ghost Zone, GOHZ; Deep photoAcclimation Zone DAZ; and Deep Biomass Zone, DBZ) from the 28 clustered regions: (a) surface [Chl*a*]sat from satellite observations, (b) iPAR at the nitracline depth (iPARNit), (c) steepness of the nitracline (mNit), and (d) difference between the DCM and the nitracline depths. DCM, Deep Chlorophyll Maximum; PAR, Photosynthetically Available Radiation.

0.31), despite apparently similar distributions. DAZ clearly presents the lowest values typical of oligotrophic conditions (median of 0.06 m^{-3} mg chl*a* m^{-3}).

3.2.2. Daily PAR at the Nitracline Depth

The daily PAR at the nitracline depth ($iPAR_{Nit}$) is a metric to assess the potential productivity associated with a DCM (Figure 9b). This value is the highest for SHAZ (median of 2.28 E m^{-2} d^{-1}). Next come DBZ and GHOZ with intermediate values (medians of 1.77 and 0.94 E m^{-2} d^{-1}, respectively), and finally DAZ with the lowest (median of 0.01 E m^{-2} d^{-1}). The four values are significantly different from one another (Mann-Witney test, highest p-value of 0.04 for DBZ and GHOZ), despite apparently close distribution of the values for the DBZ, SHAZ and GHOZ groups.

3.2.3. Nitracline Steepness

Nitracline steepness is a proxy for the intensity of the vertical diffusive nitrate flux from enriched deep layers toward the surface (Figure 9c). It is highest for DBZ (median of 0.29 µmol NO3 m^{-1} m^{-3}) and SHAZ (median of 0.10 µmol NO3 m^{-1} m^{-3}), followed by GHOZ (median of 0.08 µmol NO3 m^{-1} m^{-3}), and finally DAZ (median of 0.04 µmol NO3 m^{-1} m^{-3}). The four values are significantly different from one another (Mann-Witney test, highest p-value of 2.9 10^{-11} for SHAZ and GHOZ), despite apparently close distribution for the SHAZ and GHOZ groups.

3.2.4. Position of the Deep Chlorophyll Maximum Depth in Relation to the Nitracline Depth

The position of the DCM with respect to the nitracline depth indicates the DCM's closeness to the nutrient resource (Figure 9d). In DBZ and SHAZ, the DCM is located below the nitracline (respectively means of 8 and 1 m). In contrast, it is above the nitracline (mean of −14 m) in GHOZ, while the DCM in DAZ is the furthest from the nitracline (mean of −39 m). The values of this metric for each of the four zones are

significantly different (Mann-Witney test, highest p-value of 1.38 10^{-8} for DBZ and SHAZ), despite apparently similar distribution for the GHOZ and SHAZ groups.

3.3. Seasonal Approach in the Stratified Zones

Key environmental conditions drive DCM dynamics in each of the four main zones (previous section). Here, we assess the seasonal variability of these drivers as a way to confirm their potential significance at even smaller temporal scales. For this purpose, we focused only on the two zones with the maximum occurrences of DCMs (Deep Biomass Zone and Deep photoAcclimation Zone, Figure 7) and chose one specific region for each group: the Atlantic SubEquatorial Waters (ASEW) for the DBZ and the North Atlantic SubTropical Gyre (NASTG) for the DAZ, both regions being located in the same oceanic basin and representative of both DCM features (supportive information: Text S8 and Figure S15). In each region and regardless of the year (Figure 10), we estimated the mean monthly depths of DCM, nitracline and 20 E m^{-2} d^{-1} isolume ($iPAR_{20}$) for representative floats (supportive information: Text S8 and Figure S16). $iPAR_{20}$ isolume was chosen because it best represents the seasonality of light availability, at a depth which is not affected by the DCM features (as the DCM interacts with low light levels, see Figure 9b). Higher iPAR values would be inexistent during the winter period.

In the NASTG, the nitracline depth remains stable throughout the year (mean of 153 m). The $iPAR_{20}$ deepens from the winter to summer solstice (mean of 16 m in December to a mean of 38 m in June), with the DCM depth following a similar trend (mean of 110 m in December to a mean of 137 m in May). The mean difference between these two depths is 94 m over the year. The spring period corresponds to the time when DCMs draw closer to the nitracline, and lead to an apparition of a peak of b_{bp} at the DCM depth (supportive information Text S9 and Figure S17).

In the ASEW, the $iPAR_{20}$ shows the same seasonal pattern as in the STG, but with a lower seasonal amplitude (mean of 22 m in December to a mean of 29 m in June). The DCM follows a different trend, shallowing from winter (mean of 52 m in January) to the end summer (mean of 40 m in September). The nitracline is located above the DCM (yearly mean of 11 m) and follows the same trend (shallows from a mean of 44 m in January to a mean of 28 m in September), reaching the $iPAR_{20}$ during summer. Strongest DCMs are however observed during the spring time (supportive information Text S9 and Figure S17). DCM and nitracline depths are globally closer to the $iPAR_{20}$ throughout the year (mean annual difference of 17 m between the DCM depth and the $iPAR_{20}$), compared to the situation in the NASTG. The dispersion of the mean DCM, $iPAR_{20}$, and nitracline depths per months is provided for the two regions in the supportive information: Table S7.

4. Discussion

This study uses the global BGC-Argo float network to assess: (1) DCM presence and types (DAMs/DBMs) at a global scale and (2) the environmental drivers prevailing in the formation and maintenance of DCMs. The conditions under which a DCM and its typology are studied here refer to the theoretical framework of the Typical Stable Water Systems (TSWS) defined by Cullen (2015): water structures presenting stable enough conditions (i.e., in terms of intensity of the stratification and endurance of the latter) to lead to the establishment of a two-layer system with nutrients depleted in the upper layer and vanishing irradiance in the deeper layer (Beckmann & Hense, 2007; Dugdale, 1967; Estrada et al., 1993; Hodges & Rudnick, 2004; Voituriez & Herbland, 1979). These two-layer systems represent a challenging environment for phytoplankton growth (Kemp et al., 2000) depending on the degree of (co-)limitation of both factors (Beckmann & Hense, 2007; Cullen, 2015; Hodges & Rudnick, 2004). The characteristics of the two fundamental resources for phytoplankton (i.e., iPAR availability in the MLD, driven by the light attenuation coefficient K_d related to the [Chl*a*], and nitracline depth and steepness) and their interaction (estimated by the iPAR at the nitracline depth) were defined for the four DCM types as well as the way in which they influence their different features (i.e., their typology, position and magnitude).

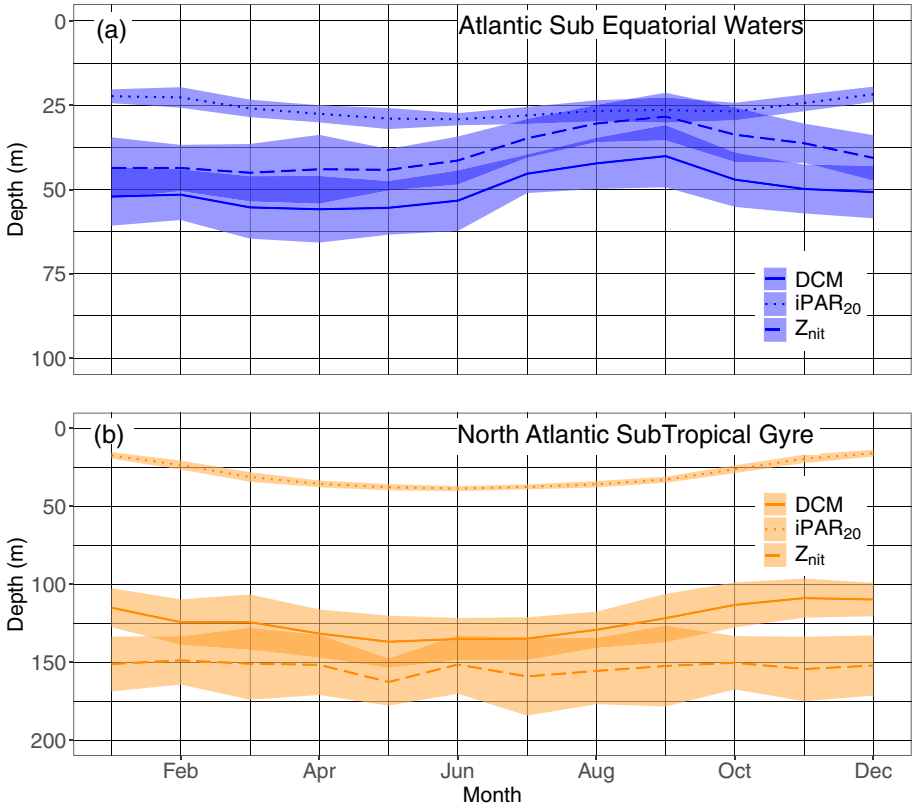

Figure 10. Mean and standard-deviation yearly climatology of the DCM depth, the depth of the iPAR 20 E m^{-2} d^{-1} isocline and the nitracline depth for the floats in the Atlantic SubEquatorial Waters (a) and in the North Atlantic Subtropical Gyre (b), respectively, representative of the Deep Biomass Zone, and of the Deep photoAcclimation Zone. DCM, Deep Chlorophyll Maximum.

4.1. Global Deep Chlorophyll Maxima Assessment

The oceanic regions sampled by BGC-Argo floats cover a wide range of trophic statuses and hydrographic regimes in the global open ocean: from stable oligotrophic regions (e.g., subtropical gyres) to highly dynamic and productive ones (e.g., north subpolar gyres), and also including semi-enclosed marginal seas (e.g., the Mediterranean Sea, Red Sea, South China Sea). A main result from this study is the identification of DAM and DBM presence in the 28 regions, attesting to the ubiquity of these features reflecting the vertical distribution of phytoplankton at a global scale.

4.1.1. Latitudinal and Seasonal Occurrence are Driven by Stratification

Even if DCMs are identified in each region of our data set, their presence and typology nevertheless exhibit strong latitudinal dependence, with nearly symmetrical patterns on either side of the Equator. A very clear contrast differentiates low-latitude systems (i.e., in equatorial/subequatorial/subtropical waters, from 0 to ~35°) from higher-latitudes ones (Figure 3). At low latitudes, DCMs emerge as an almost inherent characteristic of [Chl*a*] profiles, with the highest occurrences recorded at 20°S; at higher latitudes (above 35°), DCMs become a rather rare feature among the measured profiles. This latitudinal delineation confirms previous observations at a regional scale (Ardyna et al., 2013; Baldry et al., 2020; Cullen, 2015; DiTullio et al., 2003; Estrada et al., 2016; Holm Hansen et al., 2004; Kawamiya et al., 2000; Mignot et al., 2014; Parslow et al., 2001; Ravichandran et al., 2012; Thushara et al., 2019). This delination is also globally coherent with the satellite-based prediction put forward by Silsbe and Malkin (2016): a gradient of increasing occurrences from the poles to the Equator. For high northern latitudes, however, the present observations reveal lower DCM occurrences than those predicted by Silsbe & Malkin.

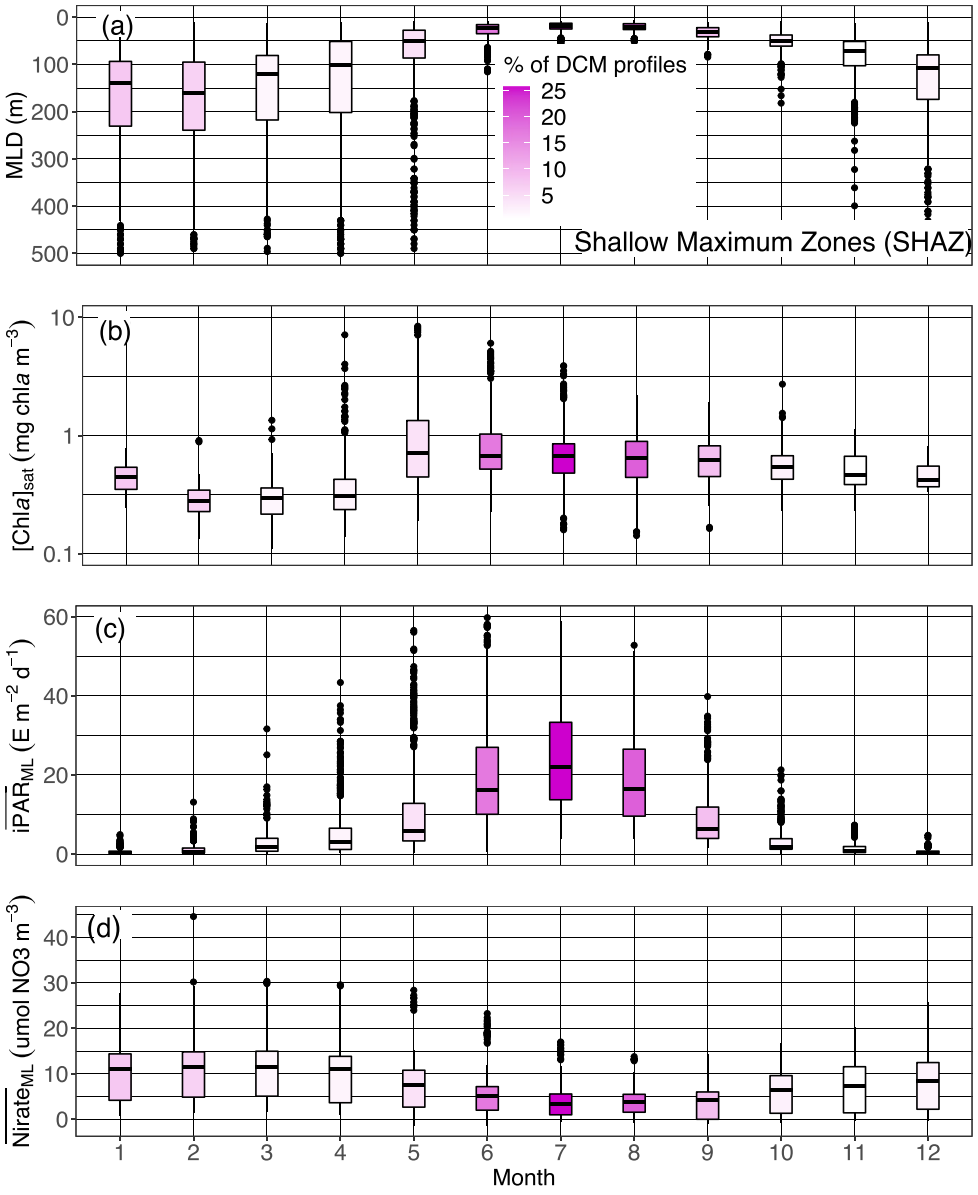

Figure 11. Quartile diagrams of (a) MLD, (b) $[Chla]_{sat}$, (c) mean daily PAR in the mixed layer ($\overline{iPAR_{ML}}$) and (d) mean nitrate concentration in the ML ($Nitrate_{ML}$) per Northern Hemisphere-phased month (regardless of the year) for SHAZ profiles with a monthly occurrence of DCM profiles color gradient. The Black Sea is excluded from this representation. DCM, Deep Chlorophyll Maximum; MLD, Mixed Layer Depth; PAR, Photosynthetically Available Radiation.

This latitudinal gradient in DCM occurrence is clearly related to a similar gradient in water-column stability throughout the year. Indeed, rather stable water conditions over time are required for the installation of a two-layer system, a prerequisite to the establishment and maintenance of a sustained DCM (Cullen, 2015; Cushing, 1989; Silsbe & Malkin, 2016). Such yearly stability is typical of permanently stratified systems, with weak variations in MLD over the year. When analyzed as a function of the latitude, the number of months in which profiles presenting a DCM feature are dominant (supportive information: Figure S18) offers an indication of the stability of stratification conditions over the year. The duration of the stratification period decreases poleward, combined with an increase in annual MLD amplitude (supportive information: Figure S18). This latitudinal dependence of stratification conditions is clearly associated with an increasing seasonality of the DCM feature (a permanent feature in subequatorial waters, a half-year period

in transition latitudes around 30°, and nearly exclusively summer occurrence above 40°, Figure 4). The latitudinal trend in DCM occurrence therefore fundamentally reflects the transition from nearly permanently stratified oligotrophic systems, to more dynamic and productive systems. The zone with the highest DCM occurrence (0–40° band) is divided into two sub-zones according to the DCM types (Figure 3): the subtropical gyres (20–40°) dominated by DAM profiles (with more photoacclimation processes) and the subequatorial zones (0–10°) dominated by DBM profiles (effective biomass accumulation).

4.1.2. Deep Chlorophyll Maxima Depth and Intensity at the Global Scale

The depth of the DCMs presents a continuous range from nearly 200 m (in the southern subtropical gyres) up to less than 20 meters deep (e.g., in the north Atlantic subpolar gyre), a range in agreement with the results of Mignot et al. (2011) (we recall here that the DCM detection method excludes the identification of DCMs shallower than 15 m).

The latitudinal distribution of DCM depth (Figure 5) mirrors the occurrence of DAMs (Figures 3 and 4): very low DAM occurrence at high latitudes, reduced occurrence at relatively shallow depths in subequatorial waters (from 0 to ∼15°), and high occurrence at great depths in subtropical areas (from ∼15 to ∼35°). This overall pattern suggests that increasing DCM depths and oligotrophic status (low $[\mathrm{Chl}a]_{sat}$, Figure 9a) are linked and associated with an increasing proportion of DCMs with a photoacclimation origin.

DCM intensities cover a continuous range (Figures 5 and 7, and supportive information: Figure S13), from less than ∼0.3 mg chl$a$ m^{-3} and $b_{bp} \sim 6\ 10^{-4}$ m^{-1} for weaker DCMs (i.e., subtropical gyres, consistent with the values described in Mignot et al., 2014) to ∼10 mg chl$a$ m^{-3} and $b_{bp} \sim 10^{-2}$ m^{-1} for the most intense (i.e., in the high northern latitudes, see supportive information, Figure S22a) with [Chl$a$] values in the range found in Baffin Bay by Martin et al. (2010).

4.1.3. Daily PAR in the Mixed Layer: An Index for the Presence of Deep Chlorophyll Maxima

Overall, the establishment and maintenance of a DCM require the daily PAR within the mixed layer $\overline{iPAR}_{ML}$, to be above a ∼15 E m^{-2} d^{-1} threshold (Figure 6). This global threshold integrated over the ML is equivalent to a threshold of 0.5 E m^{-2} d^{-1} at the base of the ML (Silsbe & Malkin, 2016) or 0.1 E m^{-2} d^{-1} at the DCM depth (Mignot et al., 2014). Note that these criteria signify that a minimum daily photon dose is required at a given depth or within a layer for a DCM to occur and be maintained, implicitly disqualifying any criteria based on relative light (e.g., euphotic zone depth defined at the depth where remains 1% of surface PAR). The $\overline{iPAR}_{ML}$ additionally presents the advantage of more mechanistically addressing the link between upper-water-column processes and the establishment of DCMs (Mignot et al., 2014), especially when considering regional and seasonal scales. The $\overline{iPAR}_{ML}$ is driven by the combination of three factors: the amount of light at the ocean surface (Morel et al., 2010); the thickness of the ML; and finally, light attenuation within the ML (Mignot et al., 2014). Surface PAR is both latitude- and season-driven: with increasing latitudes, the surface iPAR becomes lower and the amplitude of the seasonal circadian cycle intensifies. Similarly, variations in ML thickness are primarily latitude- and season-driven (de Boyer Montégut et al., 2004; Kara et al., 2003). Light attenuation within the mixed layer is regulated by the concentration of optically significant substances which, in the open ocean, consist of phytoplankton and covarying material (e.g., non-algal particles, colored dissolved organic matter). The $[\mathrm{Chl}a]_{sat}$, proxy of the trophic status within the upper layer, spans nearly two orders of magnitude (0.01–1 mg chl$a$ m^{-3}, Figure 9a and supportive information: Figure S14), whose upper range roughly corresponds to the surface $[\mathrm{Chla}]_{sat}$ threshold above which no DCM can develop, essentially because of light limitation. The DCM depth is also related to $[\mathrm{Chl}a]_{sat}$ (supportive information: Text S7 and Figure S14), which confirms that the establishment and maintenance of a DCM at a given depth require a minimum daily photon dose, which in turn is controlled by upper-ocean processes. It is interesting to also note that through photoacclimation, phytoplankton regulates chlorophyll content within the ML, and consequently exerts a feedback mechanism on light attenuation. Indeed, under low $\overline{iPAR}_{ML}$ (e.g., winter), [Chl$a$] content per phytoplankton biomass in the ML is higher, and the inverse applies for for high $\overline{iPAR}_{ML}$ (Letelier et al., 1993; Mignot et al., 2014; Winn et al., 1995). In other words, physically driven mechanisms (MLD, surface PAR) of light availability within (and below) the ML are amplified by phytoplankton photoacclimation. Physical and biological processes can thus work together to control the potential light available for DCM development at depth over a range of conditions falling between two

well-characterized endpoints. In high-latitude environments, either a deep ML and low light in winter or surface bloom in spring-summer will drastically lower the $\overline{iPAR}_{ML}$ (Wroblewski, 1989). Conversely, in subequatorial and subtropical waters, these three factors will be more favorable to higher and more stable levels of $\overline{iPAR}_{ML}$, especially during summer months (similar to what was shown by Silsbe and Malkin (2016), looking at the iPAR at the MLD). In between these two situations there exist a multitude of regional and seasonal nuances that preclude the establishment of DCMs and that will be further examined in following sections.

4.2. High-Latitude Deep Chlorophyll Maxima Systems

The clustering of regions on the basis of DCM characteristics (intensity, depth and typology of the occurrence) condenses the above observations into four typological groups (Figure 7). These groups define four representative zones whose global distribution essentially follows a latitudinal pattern (Figure 8): the high latitudes in both hemispheres, where DCM occurrence is weak, and low-latitude stratified areas, with two zones, respectively, dominated by DAM and DBM profiles.

4.2.1. SHAZ: Sporadic and Event-Driven Deep Chlorophyll Maxima

The so-called Shallow Maxima Zone (SHAZ) gathers most high-latitude regions in the north hemisphere (except for Baffin Bay, classified in the Deep Biomass Zone region), and the Black Sea. Except in the case of the latter, the DCM here exhibit four main characteristics, being: temporally restricted to a few summer months (Figures 4 and 7, and supportive information: Figures S20 and S21); intense (~2 mg chl$a$ m^{-3}); shallow (~35 m); and still rarely occurring over this period (<25%, Figure 7c). They occur exclusively in late spring and summer and correspond to mesotrophic to eutrophic water types, with higher $[\text{Chl}a]_{\text{sat}}$ (~0.6 mg chl$a$ m^{-3}, Figure 9a), observations that confirm previous assessments of summer DCM occurrence in high-latitude environments of the Northern Hemisphere (Anderson, 1969; Ardyna et al., 2013; Kawamiya et al., 2000; Martin et al., 2010; Richardson et al., 2000). These regions are characterized by strong seasonality in physical forcing and biogeochemical response, that establish conditions preventing DCM development in other seasons (e.g., winter deep mixing, spring blooms, rapid surface irradiance decrease and deepening of the mixed layer in autumn). As a consequence, only a restricted time period around the summer solstice allows DCM development. Here, the DCMs appear to be associated with very shallow MLDs (Figure 11a) which, combined with the bloom's decline at the surface (allowing more light penetration at depth) (Figure 11b), ultimately results in a high $\overline{iPAR}_{ML}$ (~25 E m^{-2} d^{-1}) (Figure 11c). Over this short time period, DCMs in SHAZ thus appear to benefit from nearly optimal environmental conditions allowing enhanced biomass (and predictably, production) (Figure 7a): high iPAR at the nitracline depth associated with a flat nitracline (Figures 9b and 9c; which suggests enhanced vertical exchanges at the nitracline depth), resulting in a DCM developing precisely at the nitracline level. The phytoplankton in these DCMs thus develop where both light and nutrient resources are synergistically favorable for growth. A question that can nevertheless be raised is why, in such favorable conditions, [Chl$a$] values remain low above in the mixed layer where nitrates are still available (Figure 11d). The likely cause is a limitation in nutrients other than nitrate, for example iron or silicate in the specific case of diatoms (respectively Hopkinson & Barbeau, 2008; Allen et al., 2005; Yool & Tyrrell, 2003).

Interestingly, DCMs observed in SHAZ are almost twice as intense as the ones in the Deep Biomass Zone, despite strong similarities in prevailing environmental conditions (Figure 9). Besides possible control by zooplankton, such differences could also potentially arise from differences in the phytoplankton species composing the DCMs in the two zones. Indeed, diatoms have often been reported in the DCM layer in SHAZ areas (Hegseth, 1998; Hill et al., 2005; Lutz et al., 2003; Martin et al., 2010; Ondrusek et al., 1991) while more mixed populations including pico-phytoplankton may shape the DBMs associated in low and mid-latitudes (respectively Takahashi & Hori, 1984; Partensky et al., 1996; Claustre et al., 1999; Acevedo-Trejos et al., 2013; and Marty et al., 2002; Lutz et al., 2003).

Finally, aside from very high biomasses, another intriguing aspect of SHAZ DCMs lies in the fact that they remain minor features during the favorable summer window. Their sparseness over this period (Figure 7) implies that conditions for their appearance are not often gathered, possibly reflecting patchiness or instability in prevailing environmental conditions.

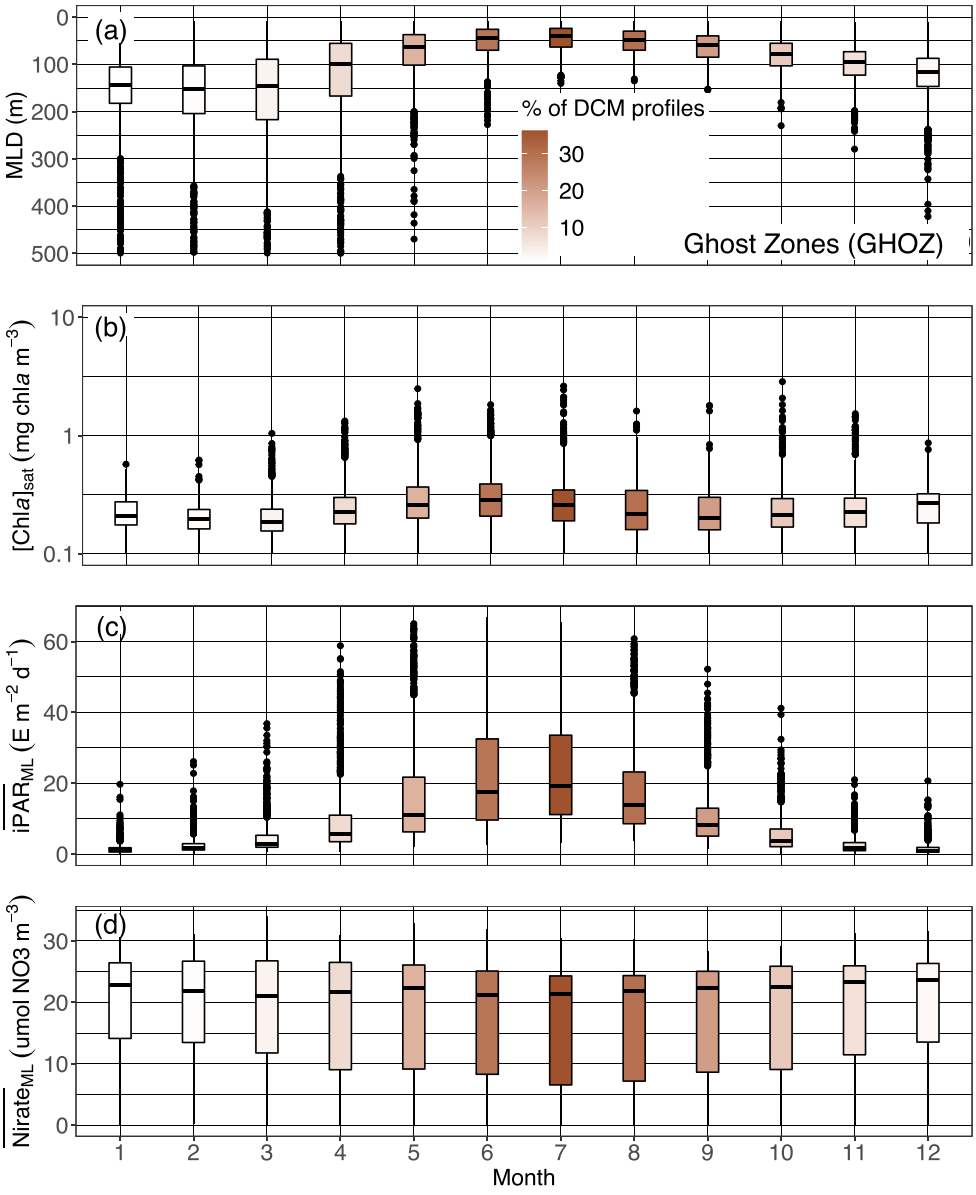

Figure 12. Quartile diagrams of (a) MLD, (b) $[Chla]_{sat}$, (c) mean daily PAR in the mixed layer ($\overline{iPAR_{ML}}$), and (d) mean nitrate concentration in the ML ($Nitrate_{ML}$) per Northern Hemisphere-phased month (regardless of the year) for GHOZ profiles with a monthly occurrence of DCM profiles (color gradient). The North Atlantic Current is excluded from this representation, as not being part of the Southern Ocean sub-regions on which our analysis essentially focuses. DCM, Deep Chlorophyll Maximum; GHOZ, Ghost Zone; MLD, Mixed Layer Depth; PAR, Photosynthetically Available Radiation.

4.2.2. GHOZ: Irregular Fertilization?

The Ghost Zone includes the four sub-regions of the Southern Ocean, and the North Atlantic Current. As for Shallow Maxima Zone, DCMs in GHOZ are restricted to a few summer months (Figure 4 and supportive information: Figures S20 and S21) and remain also rare during this period. They differ by being deeper (64 vs. 37 m) and less intense (1.4 vs. 2.4 mg chl*a* m^{-3}) (Figure 7). Those deeper depths leads to the integration of the North Atlantic Current in the GHOZ cluster rather than to the SHAZ one (supportive information: Figure S22b). Most of all, it appears that nitrate is not the limiting nutrient in the GOHZ (Figure 12d). Indeed, GHOZ cluster is dominated by profiles from the Southern Ocean, which is characterized by iron-limit-

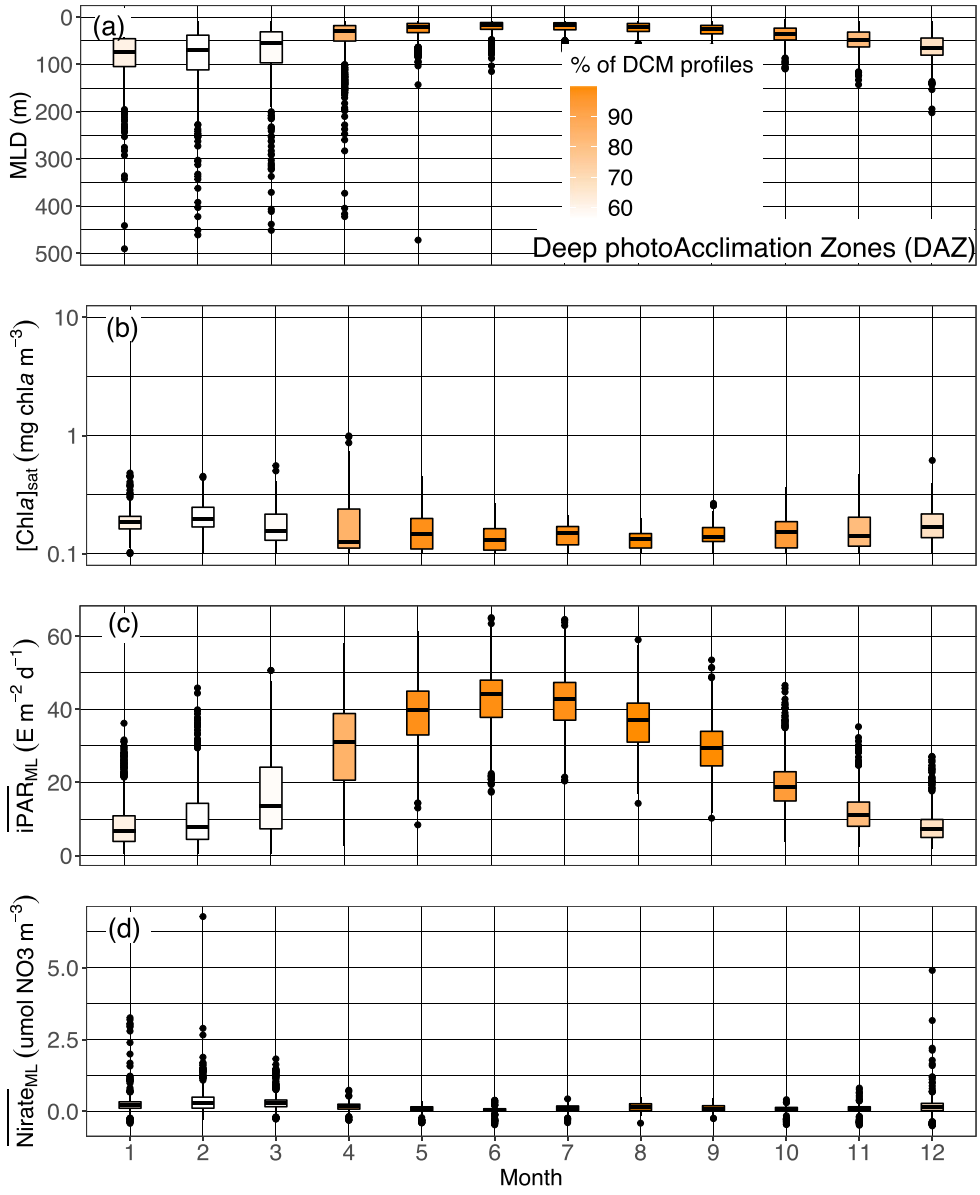

Figure 13. Quartile diagrams of (a) MLD, (b) [Chl*a*]$_{sat}$, (c) mean daily PAR in the mixed layer ($\overline{iPAR_{ML}}$), and (d) mean nitrate concentration in the ML ($Nitrate_{ML}$) per Northern Hemisphere-phased month (regardless of the year) for DAZ profiles with a monthly occurrence of DCM profiles (color gradient). DAZ, Deep photoAcclimation Zone; DCM, Deep Chlorophyll Maximum; GHOZ, Ghost Zone; MLD, Mixed Layer Depth; PAR, Photosynthetically Available Radiation.

ed high-nutrient low-chlorophyll waters (Martin et al., 1994). Iron limitation implies less productive surface waters (compare Figure 12b with Figure 11b) but nevertheless the $\overline{iPAR_{ML}}$ in summer for GHOZ remains 20% lower than for SHAZ (Figures 11c and 12c) just as the iPAR at the nitracline is 30% lower (Figure 9b). This weaker light availability results from the mixed layer being on average deeper in summer months (Figures 11a vs. 12a). Light conditions for developing and maintaining a DCM are therefore less favorable for the GHOZ cluster. On top of this light limitation, iron limitation results in the nitracline depth not being the appropriate reference to define the depth horizon where nutrient resources are sufficient for phytoplankton growth. Rather, the effective depth for favorable nutrient growth conditions is the iron-cline, expectedly located deeper (Klunder et al., 2011). In other words, in GHOZ, contrary to the situation in SHAZ, phytoplankton developing at DCMs are potentially limited by both light and nutrients.

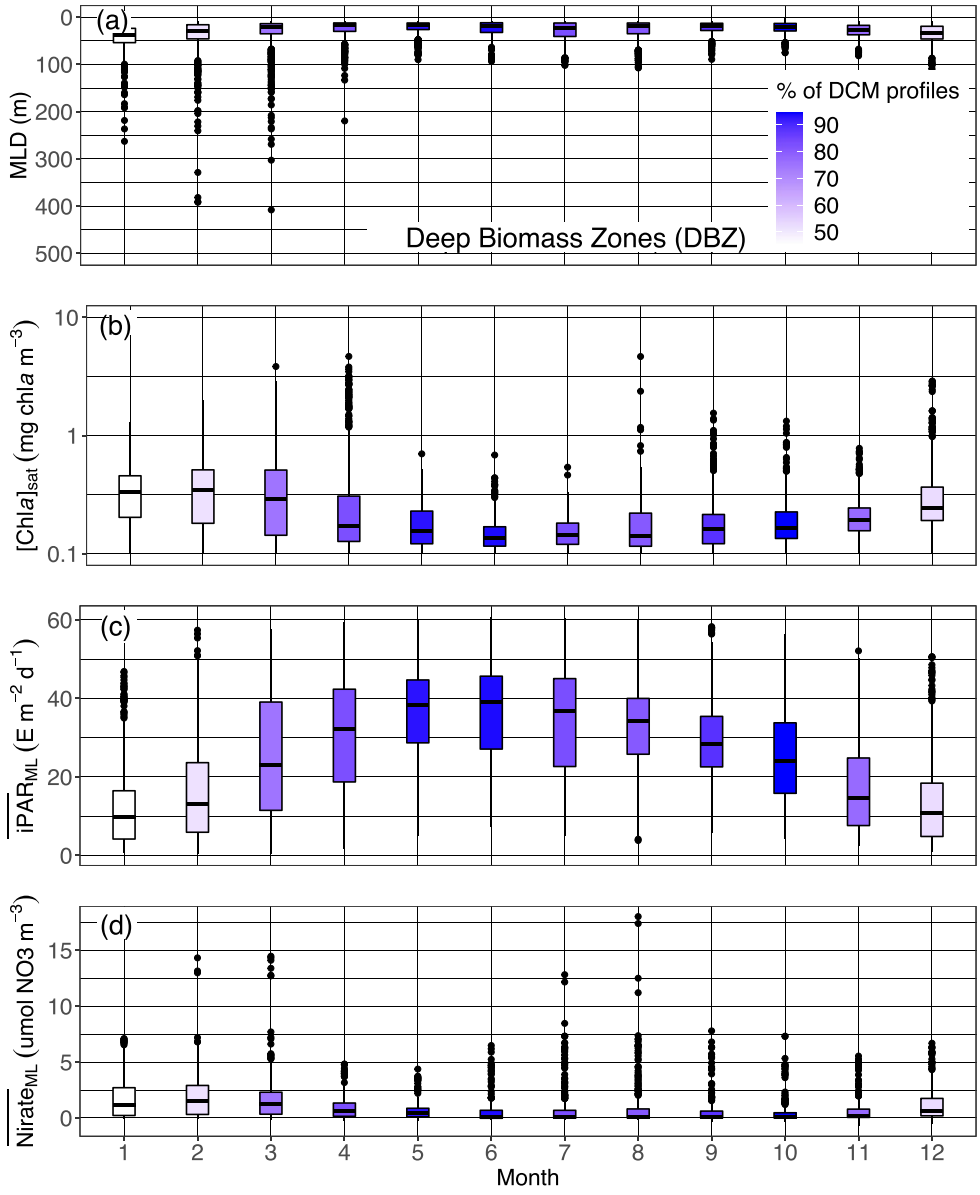

Figure 14. Quartile diagrams of (a) MLD, (b) $[Chla]_{sat}$, (c) mean daily PAR in the mixed layer ($\overline{iPAR_{ML}}$), and (d) mean nitrate concentration in the ML ($Nitrate_{ML}$) per Northern Hemisphere-phased month (regardless of the year) for DBZ profiles with a monthly occurrence of DCM profiles (color gradient). Baffin Bay is excluded from this representation. DBZ, Deep Biomass Zone; DCM, Deep Chlorophyll Maximum; MLD, Mixed Layer Depth; PAR, Photosynthetically Available Radiation.

Several studies have reported more or less persistent and recurrent DCM occurrence, mostly during the summer period, in various regions of the Southern Ocean (Armand et al., 2008; Baldry et al., 2020; Holm-Hansen et al., 2005; Parslow et al., 2001; Quéguiner, 2001; Tripathy et al., 2015; Westwood et al., 2011). The three generic reasons advanced for DCM sparseness in the SHAZ (episodic wind events, mesoscale enrichment of upper layer or control by zooplankton) also apply to this zone. In addition, several reasons more specific to the GHOZ cluster can also be advanced. First, sparse DCMs possibly originate from the local alleviation of iron limitation thanks to specific enrichments, through a variety of possible mechanisms. These mechanisms include ice retreat in the Antarctic Southern Zone/Seasonal Ice Zone (Cailliau et al., 1999; Garibotti et al., 2003), inputs from coastal shelves (Garibotti et al., 2003; Graham et al., 2015),

input of enriched-iron water layers (Holm-Hansen et al., 2005), the vicinity of southern islands (Armand et al., 2008; Blain et al., 2008), shallow bathymetries (Ardyna et al., 2017) or hydrothermal vents (Ardyna et al., 2019). Second, sparse DCMs might have a more biologically driven origin linked to phytoplankton communities, their specific adaptation to these local niches and survival strategies. Many studies report a dominance of diatoms in the composition of DCMs (Armand et al., 2008; Gomi et al., 2010; Parslow et al., 2001; Quéguiner, 2001). Some large diatoms observed may be residual of a surface bloom that faced nutrient-limiting conditions (iron and/or silica, Armand et al., 2008; Parslow et al., 2001), and then either faced a change in sinking rate with depth, or regulated their buoyancy when encountering more favorable layers (Acuña et al., 2010; Fisher & Harrison, 1996; Waite & Nodder, 2001). Deep layers enriched by active phytoplankton can also result from subduction of a surface bloom (Bathmann et al., 1997; Llort et al., 2018; Wright & Van den Enden, 2000). Quéguiner (2001) also described DCM layers resulting from an accumulation of phytoplankton detritus. Other observations describe a shift in the community between the mixed layer and the DCM, and suggest differences in how communities adapt to environmental conditions (Gomi et al., 2010; Kopczynska et al., 2001; Parslow et al., 2001; Tripathy et al., 2015). This variability may also contribute to explaining why no clear-cut environmental feature allows differentiation between the DBM and DAM profiles.

The Southern Ocean, which dominates the GHOZ cluster, is a complex environment, with a large variety of hydrological conditions, associated physical forcing and a resulting biogeochemical response. While the present analysis certainly reveals fundamental DCM features and their possible causes, more specific nuances and their associated drivers are yet to be better observed and documented, possibly with additional measurements and derived metrics and proxies.

4.3. Stratified Systems: From Photoacclimated to Productive Deep Horizons

Stratified systems are represented by the Deep photoAcclimation Zone (DAZ) and Deep Biomass Zone (DBZ) groups, where DCMs are generally permanent features. Except for some locations (Mediterranean Sea and Baffin Bay, where DCMs occur at specific seasons, supportive information: Text S10), this yearly stability directly reflects the permanently stratified conditions prevailing at those low and middle latitudes. These conditions lead to a lasting ecological equilibrium at the DCM depth for both zones. However, their respective environmental constraints lead to two highly contrasting responses in their DCM characteristics.

4.3.1. DAZ: The Photoacclimation-Driven Deep Chlorophyll Maxima

The Deep photoAcclimation Zone group gathers most oligotrophic regions in our database: the five subtropical gyres, the Eastern Mediterranean Sea, and the Archipelagos area. These regions have in common deep, weak and mostly photoacclimated DCMs. The oligotrophic character of these regions appears in their low $[\mathrm{Chl}a]_{\mathrm{sat}}$ values (Figure 9a), indicating weak surface primary production (Longhurst et al., 1995; Morel & Berthon, 1989).

The deepest DCMs are found in the southern Pacific and subtropical gyres, confirming the observations made by Pérez et al. (2006) and Mignot et al. (2014) regarding northern gyres. Both Pacific and Atlantic southern subtropical gyres show lower $[\mathrm{Chl}a]_{\mathrm{sat}}$ values (supportive information: Figure S23b), the lowest being in the Pacific, as consistent with Claustre, Huot, et al. (2008) and Ras et al. (2008). As the nitracline is generally deep, it is never eroded by winter mixing, with the result that nutrient inputs into the upper layers are essentially driven by vertical diffusivity through the nutricline, which can sometimes be modified by local physical features (McGowan & Hayward, 1978; Lewis et al., 1986; Letelier et al., 2004). The water clarity of upper layers (e.g., Morel, Gentili, et al., 2007) resulting from these low nutrient fluxes leads to high levels of $\overline{iPAR}$ in the mixed layer, which combined with permanent stratification at those latitudes (supportive information: Figure S18), gather favorable conditions for the development and maintenance of DCMs at great depths. This deep DCM position nevertheless implies low light availability (e.g., see iPAR at the nitracline depth, Figure 9b). In addition, the location of this DCM far above the nitracline (Figures 9d and 10b), and the marked steepness of the latter (Figure 9c) (conversely to what is observed in the three other zones), reflect strong nutrient limitation and weak nutrient fluxes. This extreme light and nutrient context explains the high proportion of DAM profiles in such oligotrophic systems, with photoacclimation processes (progressive increase of [Chl*a*] from surface to DAM depth, but not associated with any increase in the POC)

being responsible for the establishment of a DCM (Claustre et al., 1999; Claustre, Sciandra, & Vaulot, 2008; Cullen, 2015; Fennel & Boss, 2003; Mignot et al., 2014). We emphasize here that the distinction between DAM and DBM is dependent on the DBM identification criterion, which was primarily defined for developping our global scale approach. A regionally tuned approach for the distinction between DAM and DBM would likely allow addressing DCM characteristics and drivers on finer spatial and temporal scales, and thus exploring with more nuances such regional differences (see supportive information: Figures S20–S23).

The seasonal evolution of DCMs and their environmental drivers (i.e., light and nutrient availability during the year in a permanently stratified system) shows that the DCM location is associated with a constant isolume (e.g., for the North Atlantic Subtropical Gyre, Figure 10b, mean of 0.07 ± 0.08 E m^{-2} d^{-1}, data not shown). The mean monthly DCM depth is more tightly coupled with the mean $iPAR_{20}$ depth (Figures 15a and 15b) than with the mean nitracline depth, from which it seems somewhat decoupled. This observation is in agreement with the observations of Letelier et al. (1993), Winn et al. (1995), and Mignot et al. (2014). The implication is that phytoplankton are positioned in the lower limit of their light range in order to have as close access to the nitracline as possible, but this positioning is constrained by the seasonality of the iPAR. In most regions, we observed an increase in the proportion of DBMs over a more or less lasting period but this rise was generally concentrated in spring-summer (Figure 4). For the North Atlantic Subtropical Gyre (supportive information: Text S9 and Figure S17), the period around the solstice is associated with an increase of [Chl*a*] and the appearance of peak of b_{bp} at the DCM depth (Eppley et al., 1988; Claustre et al., 1999; Claustre, Sciandra, & Vaulot, 2008; Letelier et al., 2004; Mignot et al., 2014). This accumulation of biomass corresponds to the crossing over of the DCM depth with the nitracline, as the photon flux becomes stronger at depth following higher intensities at the ocean surface and within the mixed layer (Figures 10b and 13c). This suggests that phytoplanktonic cells reach a sufficient level of nutrients to start thriving (Anderson, 1969; Beckmann & Hense, 2007; Gong et al., 2015; Hense & Beckmann, 2008; Letelier et al., 2004; Mignot et al., 2014; Varela et al., 1994), as also revealed by progressive erosion of the nitracline supported by a decreasing trend of nitracline steepness until late summer (supportive information: Figure S24). The shallowing of the photon flux in autumn and winter draws away and decouples the DCM from the nitracline. As described by Mignot et al. (2014), the reduction of the photon flux at the DCM during winter is due to a combination of seasonal fluctuation of surface irradiance and phytoplankton photoacclimation (increasing their internal pigment concentration) in the deepening ML, contributing to the enhancement of light attenuation.

The magnitudes of [Chl*a*] and b_{bp} in oligotrophic DCMs are globally low (Figure 5). This can be explained both by a restrictive environment for nutrient resources and phytoplankton growth, and by the dominance of picophytoplanktonic cells (i.e., *Synechococcus*, *Plochlorococcus*, and picoeucaryotes) in the DCMs (Bouman et al., 2011; Claustre et al., 1999; Furuya & Marumo, 1983; Eppley et al., 1988; Liu et al., 1997; Partensky et al., 1996; Zhang et al., 2008), whose biomass is kept stable by microzooplankton grazing (Cullen et al., 1992).

4.3.2. DBZ: An Optimal Productive Niche Driven by Hydrodynamics

The Deep Biomass Zone group includes all equatorial and subequatorial regions, along with the Western Basin of the Mediterranean Sea, the Red Sea, and Baffin Bay. It is the zone where the occurrence of DBM profiles is the most elevated in terms of their proportion of DCMs (Figure 7d), and these persist throughout most of the year (depending on the region: supportive information: Figure S21). DBMs are found all year around in the equatorial and northern subequatorial waters, and progressively around the summer solstice for the other regions (supportive information: Figure S21). Compared to Deep photoAcclimation Zone, DBZ maxima features are stronger and shallower (Figures 7a and 7b), as a result of more mesotrophic characteristics (i.e., more intense $[Chla]_{sat}$, Figures 9b and 14b). They are also under more active hydrodynamical influence (closer to coastal and/or current systems) than the subtropical gyres (Mann & Lazier, 2006). As in the case of the Shallow Maxima Zone, the environmental metrics (Figure 9) characterize potential favorable growth conditions at the DCM depth: high iPAR values at the nitracline depth, a DCM position slightly above the nitracline and a very flat nitracline revealing an enhanced gradient favoring upward diffusivity fluxes. Indeed, these criteria suggest an optimal crossover of nutrient and light fields for the DCM communities to thrive. The lasting character of the DBM features also suggests the stability of the systems, with maintenance of a steady state in both biological and chemical exchanges. Unlike the DAZ, the DBZ have

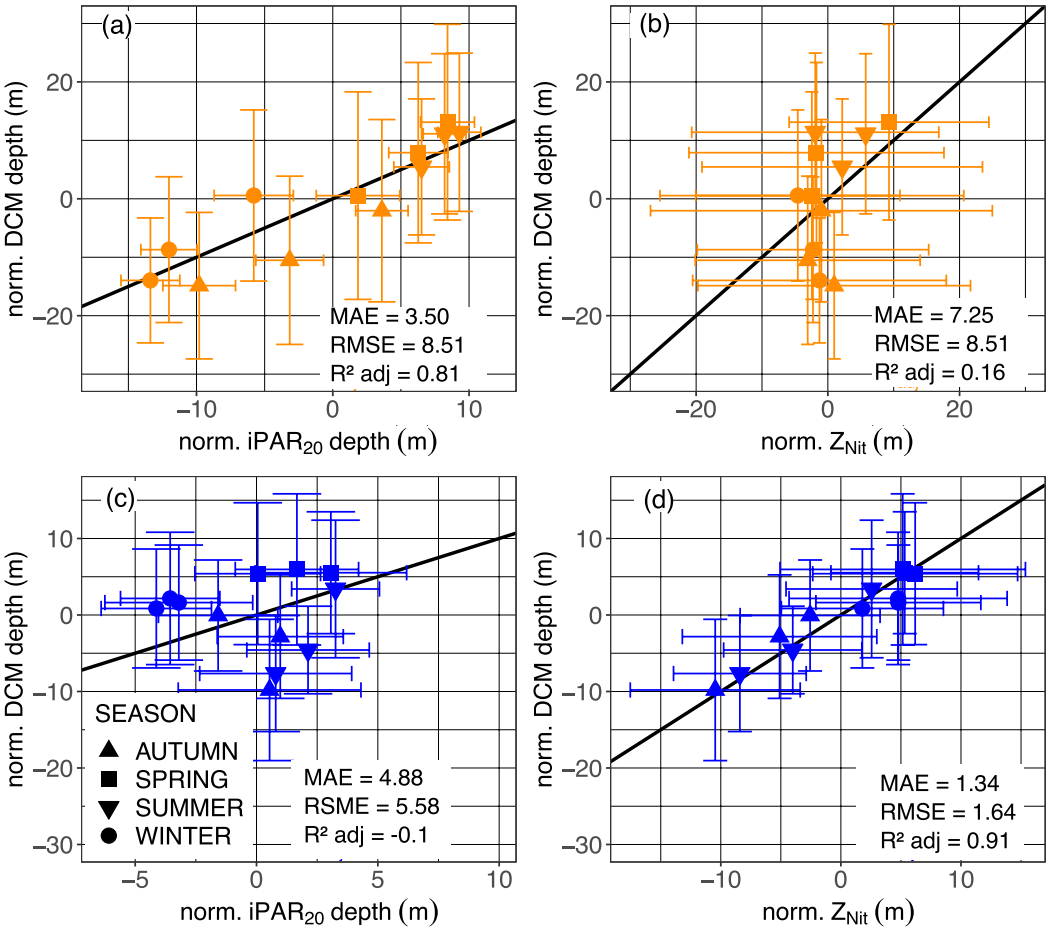

Figure 15. Normalized monthly mean DCM depth (a), (c) as a function of the normalized monthly mean depth of the iPAR 20 E m^{-2} d^{1} isocline and (b), (d) as a function of the normalized monthly mean depth of the nitracline for the representative floats of DAZ (orange, (a), (b)), and DBZ (blue, (c), (d)). The black line represents the 1:1 reference. The depth normalization procedure is described in supportive information: Text S9. DAZ, Deep photoAcclimation Zone; DCM, Deep Chlorophyll Maximum; PAR, Photosynthetically Available Radiation.

DCM depths related more to the nitracline than to light availability: the Atlantic SubEquatorial Waters (ASEW) example presents a tight coupling of the DCM depth with the nitracline depth, independently of light seasonality (Figures 10a, 15c and 15d). This correlation of the nitracline and DCM depths confirms the observations of Herbland and Voituriez (1979) and Cullen and Eppley (1981). DCM depth and nitracline manifestly follow the seasonal pattern of the MLD (supportive information: Figure S25), which suggests a tight coupling of biological and hydrological dynamics.

The present description of DBZ is consistent with mesotrophic conditions of the typical stable water structure (TSWS) framework, which show close and stable coupling between biological and physical processes and lead to biomass accumulation (Cullen, 2015; Herbland & Voituriez, 1979; Varela et al., 1992). The persistence of the DBM at an optimal light layer depends on a nearly constant input of nutrients that is not exhausted by phytoplankton consumption (Fairbanks & Wiebe, 1980; Jamart et al., 1977; Sharples & Tett, 1994; Varela et al., 1994). This continuous inflow from the deep nutrient-enriched layer may result from intense vertical diffusivity, combined with or enhanced by local and/or episodic features such as upwelling (Liu et al., 1997; Murty et al., 2000; Thushara et al., 2019; Vinogradov, 1981), turbulent mixing (Herbland et al., 1987; Herbland & Voituriez, 1979; Kaiser & Postel, 1979; Liccardo et al., 2013; McGowan & Hayward, 1978), weather influence (Murty et al., 2000; Sugimoto et al., 1995), or local hydrological pertur-

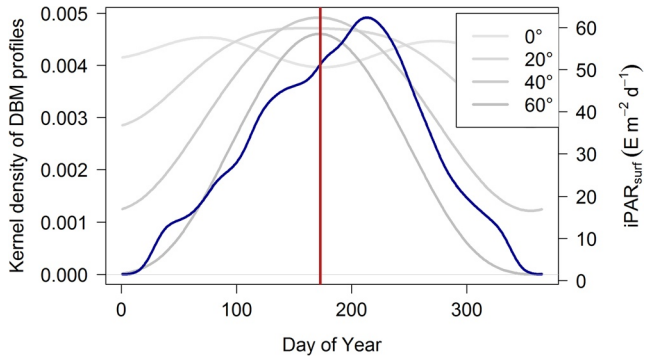

Figure 16. Density distribution of all DBM profiles as a function of the day of the Northern Hemisphere-phased year (blue line) with surface iPAR at 0°, 20°, 40° and 60° latitude (gray lines). The vertical red line corresponds to the summer solstice. DBM, Deep Biomass Maximum.

bations (e.g., mescoscale features, Brown et al., 2008; Cullen et al., 1983; Huang & Xu, 2018; Lévy, 2003; McGillicuddy & Robinson, 1997; F. F. Pérez et al., 2003; Steele & Yentsch, 1960).

5. Summary and Conclusion

This study took advantage of the global network of BGC-Argo floats to assess DCM presence and characteristics at a global scale in the open ocean. A method for the detection and classification of DCMs was developed, based on a homogeneous data set of Chl*a* and b_{bp} fluorescence (the respective proxies for [Chl*a*] and [POC]) vertical profiles. Once detected, the DCMs were further classified either as features of photoacclimation (DAM) or the accumulation of phytoplankton biomass (DBM). The 28 sampled regions were then further divided into four groups based on the DCMs' main characteristics.

DCMs were found to be a ubiquitous feature in all 28 sampled regions, as is globally consistent with previous localized observations, hence allowing some generalization into a global context. Since the occurrence of DCMs as well as their associated biomass and vertical features clearly appear to be seasonally and regionally dependent, it is possible to classify DCMs into four representative groups based on their main characteristics.

DCM distribution is latitudinally and seasonally driven. DCMs are permanent and frequent features at low latitudes (i.e., equatorial/subequatorial and subtropical waters, from 0 to ~35°, represented by the Deep photoAcclimation Zone and Deep Biomass Zone groups) while being sparse and generally associated with end of spring-summer appearances at higher latitudes (represented by the Shallow Maxima Zone and Ghost Zone groups). This observation confirms the importance of water-mass stability (whose endurance depends on the latitude) as a first-order driver to allow the establishment of a DCM feature.

DCMs require a minimum light level in the mixed layer (conditioned by the MLD depth and [Chl*a*] in its layer) as a necessary (but not, by itself, sufficient) condition for their development and maintenance. The maximum occurrence of DCMs, and more particularly DBMs, appears to follow the summer solstice by ~50 days (Figure 16). In temperate and high-latitude zones, this period not only corresponds to an increase in surface solar irradiance but also post-bloom conditions where the upper layer progressively loses its organic material, hence allowing deeper penetration of light. At low latitudes (e.g., subtropical waters), the summer-solstice period corresponds to the lowest [Chl*a*] content in the upper layer, also favoring the deepening of isolumes.

The latitudes with a high occurrence of DCMs (from 0 to 30°) are divided into two subzones in relation to biomass accumulation at the DCM, and the prevailing mechanisms behind it (DBZ and DAZ). Oligotrophic regimes (corresponding mostly to subtropical waters, at around 25°) are generally marked by significant DAM frequency with a low level of biomass accumulation. Their annual depth cycles are driven by light availability (as shown by Letelier et al., 2004; Mignot et al., 2014), and their intensity may increase as they reach out for the deep nitracline in the summer period. Meanwhile, equatorial and subequatorial latitudes present frequent biomass-accumulation features during the year. Their dynamics rely on nutrient inputs from layers below into favorable light levels at depth, as described by Herbland and Voituriez (1979).

In low-latitude areas (below 30°), both DBZ and DAZ have the potential to significantly contribute to global primary production. This is due to permanent and sometimes relatively intense biomass (especially below 15° latitude, Figure 5b) associated with DCMs as well as the global coverage of these zones (>60% of the ocean surface for oligotrophic regions alone, Longhurst et al., 1995). Observations of DCM features in such low-latitude environments need to be further reinforced, as observational gaps subsist, especially in the southern subequatorial waters of the Pacific and Atlantic basins. Also, most equatorial profiles (i.e., below 5° latitude) were acquired in the Indian Ocean. Additional data at low latitudes, especially in the two other oceanic basins, should offer insights into the spatial extent of DBMs, as such equatorial systems may differ from subequatorial ones through specific hydrological features in the divergence zone (Claustre et al., 1999;

Estrada et al., 2016; Mann & Lazier, 2006). Importantly, more in-depth investigations are required to evaluate the impact of mesoscale eddies in oligotrophic gyres as mechanisms fueling the DCM depth horizon with nutrients, hence favoring local DBM formation in regions that were classified as DAZ in the present study (Brown et al., 2008; Letelier et al., 2004; Vaillancourt et al., 2003).

At temperate and high latitudes (above 35°), DCMs are sparse even if optimal environmental conditions appear to be present for their appearance around the solstice period. These seasonal DCMs are more intense than those observed at low latitudes, some of them possibly being byproducts of surface spring blooms slowly exported to DCMs. The difficulty of making more generalizations on the conditions that prevail in the development of these types of DCMs is likely to be due to the diversity and patchiness of possible driving processes in these dynamic areas, including the time of the surface bloom's initiation and disappearance, variability of the stratification duration, and grazing pressure. Importantly, the constraints of other limiting factors (e.g., iron, silicate) also need to be evaluated, considering that many regions at these high latitudes are iron-limited (aside from the fact that the North Pacific area is still weakly instrumented by BGC-Argo floats). Further investigations taking into account other nutrients apart from nitrates, and the prospect of new insights into zooplankton communities thanks to new sensors embedded on BGC floats, could improve understanding about the mechanisms constraining DCM dynamics in these regions (Chai et al., 2020; Haëntjens et al., 2020).

Data Availability Statement

All other original data are available from the Argo Global Data Assembly Center (ftp://ftp.ifremer.fr/ifremer/argo). These data were collected and made freely available by the International Argo Program and the national programs that contribute to it: (http://www.argo.ucsd.edu, https://www.ocean-ops.org). The Argo Program is part of the Global Ocean Observing System. The databases produced for this paper are available at the following: https://doi.org/10.17882/77207.

Acknowledgments
This study is a contribution to the following projects: remOcean (European Research Council, Grant agreement 246777); REFINE (European Research Council, Grant agreement 834177); AtlantOS (European Union's Horizon 2020 research and innovation program, Grant 2014-633211); NAOS (Agence Nationale de la Recherche, grant agreement J11R107-F); SOCLIM (BNP Foundation); BGC-Argo-France (CNES-TOSCA). Haili Wang is acknowledged for giving access to data from three floats in the South China Sea. The authors wish to thank the Argo Data Management team (ADMT) and the BGC-Argo Data Management team (BGC ADMT).

References

Acevedo-Trejos, E., Brandt, G., Merico, A., & Smith, S. L. (2013). Biogeographical patterns of phytoplankton community size structure in the oceans. *Global Ecology and Biogeography*, *22*(9), 1060–1070. https://doi.org/10.1111/geb.12071

Acuña, J. L., López-Alvarez, M., Nogueira, E., & González-Taboada, F. (2010). Diatom flotation at the onset of the spring phytoplankton bloom: An in situ experiment. *Marine Ecology Progress Series*, *400*, 115–125. https://doi.org/10.3354/meps08405

Allen, J. T., Brown, L., Sanders, R., Moore, C. M., Mustard, A., Fielding, S., et al. (2005). Diatom carbon export enhanced by silicate upwelling in the northeast Atlantic. *Nature*, *437*(7059), 728–732. https://doi.org/10.1038/nature03948

Anderson, G. C. (1969). Subsurface chlorophyll maximum in the Pacific ocean. *Limnology & Oceanography*, *14*(3), 386–391. https://doi.org/10.4319/lo.1969.14.3.0386

Antoine, D., André, J.-M., & Morel, A. (1996). Oceanic primary production: 2. Estimation at global scale from satellite (Coastal Zone Color Scanner) chlorophyll. *Global Biogeochemical Cycles*, *10*(1), 57–69. https://doi.org/10.1029/95gb02832

Ardyna, M., Babin, M., Devred, E., Forest, A., Gosselin, M., Raimbault, P., & Tremblay, J. É. (2017). Shelf-basin gradients shape ecological phytoplankton niches and community composition in the coastal Arctic Ocean (Beaufort Sea). *Limnology & Oceanography*, *62*(5), 2113–2132. https://doi.org/10.1002/lno.10554

Ardyna, M., Babin, M., Gosselin, M., Devred, E., Bélanger, S., Matsuoka, A., & Tremblay, J. É. (2013). Parameterization of vertical chlorophyll a in the Arctic Ocean: Impact of the subsurface chlorophyll maximum on regional, seasonal and annual primary production estimates. *Biogeosciences*, *10*(1), 1345–1399. https://doi.org/10.5194/bg-10-4383-2013

Ardyna, M., Lacour, L., Sergi, S., d'Ovidio, F., Sallée, J. B., Rembauville, M., et al. (2019). Hydrothermal vents trigger massive phytoplankton blooms in the Southern Ocean. *Nature Communications*, *10*(1), 1–8. https://doi.org/10.1038/s41467-019-09973-6

Argo. (2020). *Argo float data and metadata from global data assembly center (Argo GDAC) – snapshot of Argo GDAC of january 2020*. SEANOE. https://doi.org/10.17882/42182#69589

Armand, L. K., Cornet-Barthaux, V., Mosseri, J., & Quéguiner, B. (2008). Late summer diatom biomass and community structure on and around the naturally iron-fertilised Kerguelen Plateau in the Southern Ocean. *Deep-Sea Research Part II: Topical Studies in Oceanography*, *55*(5–7), 653–676. https://doi.org/10.1016/j.dsr2.2007.12.031

Baldry, K., Strutton, P. G., Hill, N. A., & Boyd, P. W. (2020). Subsurface Chlorophyll-a Maxima in the Southern Ocean. *Frontiers in Marine Science*, *7*, 671. https://doi.org/10.3389/fmars.2020.00671

Banse, K. (1987). Clouds, deep chlorophyll maxima and the nutrient supply to the mixed layer of stratified water bodies. *Journal of Plankton Research*, *9*(5), 1031–1036. https://doi.org/10.1093/plankt/9.5.1031

Barbieux, M., Uitz, J., Gentili, B., Pasqueron De Fommervault, O., Mignot, A., Poteau, A., et al. (2019). Bio-optical characterization of subsurface chlorophyll maxima in the Mediterranean Sea from a Biogeochemical-Argo float database. *Biogeosciences*, *16*(6), 1321–1342. https://doi.org/10.5194/bg-16-1321-2019

Bathmann, U. V., Scharek, R., Klaas, C., Dubischar, C. D., & Smetacek, V. S. (1997). Spring development of phytoplankton biomass and composition in major water masses of the Atlantic sector of the Southern Ocean. *Deep-Sea Research Part II: Topical Studies in Oceanography*, *44*(1–2), 51–67. https://doi.org/10.1016/s0967-0645(96)00063-x

Beckmann, A., & Hense, I. (2007). Beneath the surface: Characteristics of oceanic ecosystems under weak mixing conditions – A theoretical investigation. *Progress in Oceanography*, *75*(4), 771–796. https://doi.org/10.1016/j.pocean.2007.09.002

Bellacicco, M., Cornec, M., Organelli, E., Brewin, R. J. W., Neukermans, G., Volpe, G., et al. (2019). Global variability of optical backscattering by non-algal particles from a biogeochemical-argo data set. *Geophysical Research Letters*, *46*(16), 9767–9776. https://doi.org/10.1029/2019gl084078

Bittig, H. C., Steinhoff, T., Claustre, H., Fiedler, B., Williams, N. L., Sauzède, R., et al. (2018). An alternative to static climatologies: Robust estimation of open ocean CO2 variables and nutrient concentrations from T, S, and O2 data using Bayesian neural networks. *Frontiers in Marine Science*, *5*, 328. https://doi.org/10.3389/fmars.2018.00328

Blain, S., Sarthou, G., & Laan, P. (2008). Distribution of dissolved iron during the natural iron-fertilization experiment KEOPS (Kerguelen Plateau, Southern Ocean). *Deep-Sea Research Part II: Topical Studies in Oceanography*, *55*(5–7), 594–605. https://doi.org/10.1016/j.dsr2.2007.12.028

Bouman, H. A., Ulloa, O., Barlow, R., Li, W. K. W., Platt, T., Zwirglmaier, K., et al. (2011). Water-column stratification governs the community structure of subtropical marine picophytoplankton. *Environmental Microbiology Reports*, *3*(4), 473–482. https://doi.org/10.1111/j.1758-2229.2011.00241.x

Brown, S. L., Landry, M. R., Selph, K. E., Jin Yang, E., Rii, Y. M., & Bidigare, R. R. (2008). Diatoms in the desert: Plankton community response to a mesoscale eddy in the subtropical North Pacific. In *Deep-sea Research Part II: Topical studies in oceanography*. https://doi.org/10.1016/j.dsr2.2008.02.012

Cailliau, C., Belviso, S., Goutx, M., Bedo, A., Park, Y., & Charriaud, E. (1999). Sedimentation pathways in the Indian sector of the Southern Ocean during a production regime dominated by regeneration. *Marine Ecology Progress Series*, *190*, 53–67. https://doi.org/10.3354/meps190053

Cetinić, I., Perry, M. J., Briggs, N. T., Kallin, E., D'Asaro, E. A., & Lee, C. M. (2012). Particulate organic carbon and inherent optical properties during 2008 North Atlantic bloom experiment. *Journal of Geophysical Research*, *117*(C6). https://doi.org/10.1029/2011JC007771

Chai, F., Johnson, K. S., Claustre, H., Xing, X., Wang, Y., Boss, E., et al. (2020). Monitoring ocean biogeochemistry with autonomous platforms. *Nature Reviews Earth & Environment*, *1*(6), 315–326. https://doi.org/10.1038/s43017-020-0053-y

Claustre, H., Huot, Y., Obernosterer, I., Gentili, B., Tailliez, D., & Lewis, M. (2008a). Gross community production and metabolic balance in the South Pacific Gyre, using a non intrusive bio-optical method. *Biogeosciences*, *5*(2), 463–474. https://doi.org/10.5194/bg-5-463-2008

Claustre, H., Johnson, K. S., & Takeshita, Y. (2020). Observing the Global Ocean with Biogeochemical-Argo. In *Annual review of Marine science*. https://doi.org/10.1146/annurev-marine-010419-010956

Claustre, H., Morel, A., Babin, M., Cailliau, C., Marie, D., Marty, J., et al. (1999). Variability in particle attenuation and chlorophyll fluorescence in the tropical Pacific: Scales, patterns, and biogeochemical implications. *Journal of Geophysical Research*, *104*(C2), 3401–3422. https://doi.org/10.1029/98jc01334

Claustre, H., Sciandra, A., & Vaulot, D. (2008). Introduction to the special section bio-optical and biogeochemical conditions in the South East Pacific in late 2004: The BIOSOPE program. *Biogeosciences*, *5*(3), 679–691. https://doi.org/10.5194/bg-5-679-2008

Cullen, J. J. (1982). The deep chlorophyll maximum: Comparing vertical profiles of chlorophyll a. *Canadian Journal of Fisheries and Aquatic Sciences*, *39*(5), 791–803. https://doi.org/10.1139/f82-108

Cullen, J. J. (2015). Subsurface chlorophyll maximum layers: Enduring enigma or mystery solved? *Annual Review of Marine Science*, *7*(1), 207–239. https://doi.org/10.1146/annurev-marine-010213-135111

Cullen, J. J., & Eppley, R. (1981). Chlorophyll maximum layers of the southern-california bight and possible mechanisms of their formation and maintenance. *Oceanologica Acta*, *4*(1), 23–32.

Cullen, J. J., Lewis, M. R., Davis, C. O., & Barber, R. T. (1992). Photosynthetic characteristics and estimated growth rates indicate grazing is the proximate control of primary production in the equatorial Pacific. *Journal of Geophysical Research*, *97*(C1), 639–654. https://doi.org/10.1029/91jc01320

Cullen, J. J., Stewart, E., Renger, E., Eppley, R. W., & Winant, C. D. (1983). Vertical motion of the thermocline, nitracline and chlorophyll maximum layers in relation to currents on the Southern California shelf (ceratium). *Journal of Marine Research*, *41*(2), 239–262. https://doi.org/10.1357/002224083788520171

Cushing, D. H. (1989). A difference in structure between ecosystems in strongly stratified waters and in those that are only weakly stratified. *Journal of Plankton Research*, *11*(1), 1–13. https://doi.org/10.1093/plankt/11.1.1

de Boyer Montégut, C., Madec, G., Fischer, A. S., Lazar, A., & Iudicone, D. (2004). Mixed layer depth over the global ocean: An examination of profile data and a profile-based climatology. *Journal of Geophysical Research*, *109*(C12), 1–20. https://doi.org/10.1029/2004jc002378

DiTullio, G. R., Geesey, M. E., Jones, D. R., Daly, K. L., Campbell, L., & Smith, W. O. (2003). Phytoplankton assemblage structure and primary productivity along 170°W in the South Pacific Ocean. *Marine Ecology Progress Series*, *255*, 55–80. https://doi.org/10.3354/meps255055

Dugdale, R. C. (1967). Nutrient limitation in the sea: Dynamics, identification and significance 1. *Limnology & Oceanography*, *12*(4), 685–695. https://doi.org/10.4319/lo.1967.12.4.0685

Eppley, R., Swift, E., Redalje, D., Landry, M., & Haas, L. (1988). Subsurface chlorophyll maximum in August-September 1985 in the CLIMAX area of the North Pacific. *Marine Ecology Progress Series*, *42*, 289–301. https://doi.org/10.3354/meps042289

Estrada, M., Delgado, M., Blasco, D., Latasa, M., Cabello, A. M., Benítez-Barrios, V., et al. (2016). Phytoplankton across tropical and subtropical regions of the Atlantic, Indian and Pacific oceans. *PloS One*, *11*(3), 1–29. https://doi.org/10.1371/journal.pone.0151699

Estrada, M., Marrasé, C., Latasa, M., Berdalet, E., Delgado, M., & Riera, T. (1993). Variability of deep chlorophyll maximum characteristics in the Northwestern Mediterranean. *Marine Ecology Progress Series*, *92*(3), 289–300. https://doi.org/10.3354/meps092289

Fairbanks, R. G., & Wiebe, P. H. (1980). Foraminifera and chlorophyll maximum: Vertical distribution, seasonal succession, and paleoceanographic significance. *Science*, *209*(4464), 1524–1526. https://doi.org/10.1126/science.209.4464.1524

Fennel, K., & Boss, E. (2003). Subsurface maxima of phytoplankton and chlorophyll: Steady-state solutions from a simple model. *Limnology & Oceanography*, *48*(4), 1521–1534. https://doi.org/10.4319/lo.2003.48.4.1521

Fisher, A. E., & Harrison, P. J. (1996). Does carbohydrate content affect the sinking rates of marine diatoms? *Journal of Phycology*, *32*(3), 360–365. https://doi.org/10.1111/j.0022-3646.1996.00360.x

Furuya, K., & Marumo, R. (1983). The structure of the phytoplankton community in the subsurface chlorophyll maxima in the western North Pacific Ocean. *Journal of Plankton Research*, *107*(3), 529–539. https://doi.org/10.1093/plankt/5.3.393

Garibotti, I. A., Vernet, M., Ferrario, M. E., Smith, R. C., Ross, R. M., & Quetin, L. B. (2003). Phytoplankton spatial distribution patterns along the western Antarctic Peninsula (Southern Ocean). *Marine Ecology Progress Series*, *261*, 21–39. https://doi.org/10.3354/meps261021

Gomi, Y., Fukuchi, M., & Taniguchi, A. (2010). Diatom assemblages at subsurface chlorophyll maximum layer in the eastern Indian sector of the Southern Ocean in summer. *Journal of Plankton Research*, *32*(7), 1039–1050. https://doi.org/10.1093/plankt/fbq031

Gong, X., Shi, J., Gao, H. W., & Yao, X. H. (2015). Steady-state solutions for subsurface chlorophyll maximum in stratified water columns with a bell-shaped vertical profile of chlorophyll. *Biogeosciences*, *12*(4), 905–919. https://doi.org/10.5194/bg-12-905-2015

Gordon, H. R., & McCluney, W. (1975). Estimation of the Depth of Sunlight Penetration in the Sea for Remote Sensing. *Applied Optics*, *14*(2), 413–416. https://doi.org/10.1364/ao.14.000413

Graham, R. M., De Boer, A. M., van Sebille, E., Kohfeld, K. E., & Schlosser, C. (2015). Inferring source regions and supply mechanisms of iron in the Southern Ocean from satellite chlorophyll data. *Deep-Sea Research Part I: Oceanographic Research Papers*, *104*, 9–25. https://doi.org/10.1016/j.dsr.2015.05.007

Gregg, W. W., & Carder, K. L. (1990). A simple spectral solar irradiance model for cloudless maritime atmospheres. *Limnology & Oceanography*, *35*(8), 1657–1675. https://doi.org/10.4319/lo.1990.35.8.1657

Haëntjens, N., Della Penna, A., Briggs, N., Karp-Boss, L., Gaube, P., Claustre, H., & Boss, E. (2020). Detecting Mesopelagic Organisms Using Biogeochemical-Argo Floats. *Geophysical Research Letters*, *47*(6). https://doi.org/10.1029/2019gl086088

Hegseth, E. N. (1998). Primary production of the northern Barents Sea. *Polar Research*, *17*(2), 113–123. https://doi.org/10.1111/j.1751-8369.1998.tb00266.x

Hense, I., & Beckmann, A. (2008). Revisiting subsurface chlorophyll and phytoplankton distributions. *Deep-Sea Research Part I: Oceanographic Research Papers*, *55*(9), 1193–1199. https://doi.org/10.1016/j.dsr.2008.04.009

Herbland, A., Le Bouteiller, A., & Raimbault, P. (1987). Does the nutrient enrichment of the equatorial upwelling influence the size structure of phytoplankton in the Atlantic Ocean? *Oceanologica Acta, Special Issue*, 115–120. https://archimer.ifremer.fr/doc/00267/37855/

Herbland, A., & Voituriez, B. (1977). Production primaire, nitrate et nitrite dans l'Atlantique tropical. 1. Distribution de nitrate et production de nitrite. *Cahiers O.R.S.T.O.M. Serie Oceanographie*, 47–55.

Herbland, A., & Voituriez, B. (1979). Hydrological structure analysis for estimating the primary production in the tropical Atlantic Ocean. *Journal of Marine Research*, *37*(1), 87–101.

Hill, V., Cota, G., & Stockwell, D. (2005). Spring and summer phytoplankton communities in the Chukchi and Eastern Beaufort Seas. *Deep-Sea Research Part II: Topical Studies in Oceanography*, *52*(24–26), 3369–3385. https://doi.org/10.1016/j.dsr2.2005.10.010

Hodges, B., & Rudnick, D. (2004). Simple models of steady deep maxima in chlorophyll and biomass. *Deep-Sea Research Part I: Oceanographic Research Papers*, *51*(8), 999–1015. https://doi.org/10.1016/j.dsr.2004.02.009

Holm-Hansen, O., & Hewes, C. D. (2004). Deep chlorophyll-a maxima (DCMs) in Antarctic waters: I. Relationships between DCMs and the physical, chemical, and optical conditions in the upper water column. *Polar Biology*, *27*(11), 699–710. https://doi.org/10.1007/s00300-004-0641-1

Holm-Hansen, O., Kahru, M., & Hewes, C. D. (2005). Deep chlorophyll a maxima (DCMs) in pelagic Antarctic waters. II. Relation to bathymetric features and dissolved iron concentrations. *Marine Ecology Progress Series*, *297*, 71–81. https://doi.org/10.3354/meps297071

Hopkinson, B. M., & Barbeau, K. A. (2008). Interactive influences of iron and light limitation on phytoplankton at subsurface chlorophyll maxima in the eastern North Pacific. *Limnology & Oceanography*, *53*(4), 1303–1318. https://doi.org/10.4319/lo.2008.53.4.1303

Huang, J., & Xu, F. (2018). Observational Evidence of Subsurface Chlorophyll Response to Mesoscale Eddies in the North Pacific. *Geophysical Research Letters*, *45*(16), 8462–8470. https://doi.org/10.1029/2018gl078408

Huisman, J., Pham Thi, N. N., Karl, D. M., & Sommeijer, B. (2006). Reduced mixing generates oscillations and chaos in the oceanic deep chlorophyll maximum. *Nature*, *439*(7074), 322–325. https://doi.org/10.1038/nature04245

Jamart, B. M., Winter, D. F., Banse, K., Anderson, G. C., & Lam, R. K. (1977). A theoretical study of phytoplankton growth and nutrient distribution in the Pacific Ocean off the northwestern U.S. coast. In *Deep-sea Research*. https://doi.org/10.1016/0146-6291(77)90498-2

Joint, I., & Groom, S. B. (2000). Estimation of phytoplankton production from space: Current status and future potential of satellite remote sensing. *Journal of Experimental Marine Biology and Ecology*, *250*(1–2), 233–255. https://doi.org/10.1016/s0022-0981(00)00199-4

Kaiser, W., & Postel, L. (1979). Importance of the vertical nutrient flux for biological production in the equatorial undercurrent region at 30°W. *Marine Biology*, *53*, 23–27. https://doi.org/10.1007/BF00391713

Kara, A. B., Rochford, P. A., & Hurlburt, H. E. (2003). Mixed layer depth variability over the global ocean. *Journal of Geophysical Research*, *108*(C3), 24–1. https://doi.org/10.1029/2000jc000736

Karl, D. M., Letelier, R. M., Hebel, D. V., Tupas, L., Dore, J., Christian, J., & Winn, C. D. (1995). Ecosystem changes in the North Pacific subtropical gyre attributed to the 1991–92 El Niño. *Nature*, *373*(6511), 230–234. https://doi.org/10.1038/373230a0

Kawamiya, M., Kishi, M. J., & Suginohara, N. (2000). An ecosystem model for the North Pacific embedded in a general circulation model. Part I: Model description and characteristics of spatial distributions of biological variables. *Journal of Marine Systems*, *25*(2), 129–157. https://doi.org/10.1016/s0924-7963(00)00012-9

Kemp, A. E. S., Pike, J., Pearce, R. B., & Lange, C. B. (2000). The "Fall dump" – A new perspective on the role of a "shade flora" in the annual cycle of diatom production and export flux. *Deep-Sea Research Part II: Topical Studies in Oceanography*, *47*(9–11), 2129–2154. https://doi.org/10.1016/s0967-0645(00)00019-9

Kiefer, D., Olson, R. J., & Holm-Hansen, O. (1976). Another look at the nitrite and chlorophyll maxima in the central North Pacific. *Deep-Sea Research and Oceanographic Abstracts*, *23*(12), 1199–1208. https://doi.org/10.1016/0011-7471(76)90895-0

Klausmeier, C. A., & Litchman, E. (2001). Algal games: The vertical distribution of phytoplankton in poorly mixed water columns. *Limnology & Oceanography*, *46*(8), 1998–2007. https://doi.org/10.4319/lo.2001.46.8.1998

Klunder, M. B., Laan, P., Middag, R., De Baar, H. J., & van Ooijen, J. C. (2011). Dissolved iron in the Southern Ocean (Atlantic sector). *Deep-Sea Research Part II: Topical Studies in Oceanography*, *58*(25–26), 2678–2694. https://doi.org/10.1016/j.dsr2.2010.10.042

Kopczynska, E. E., Dehairs, F., Elskens, M., & Wright, S. (2001). Phytoplankton and microzooplankton variability between the Subtropical and Polar Fronts south of Australia: Thriving under regenerative and new production in late summer. *Journal of Geophysical Research*, *106*(C12), 31597–31609. https://doi.org/10.1029/2000jc000278

Lacour, L., Ardyna, M., Stec, K. F., Claustre, H., Prieur, L., Poteau, A., et al. (2017). Unexpected winter phytoplankton blooms in the North Atlantic subpolar gyre. *Nature Geoscience*, *10*(11), 836–839. https://doi.org/10.1038/ngeo3035

Lavigne, H., D'Ortenzio, F., Ribera D'Alcalà, M., Claustre, H., Sauzède, R., & Gacic, M. (2015). On the vertical distribution of the chlorophyll a concentration in the Mediterranean Sea: A basin-scale and seasonal approach. *Biogeosciences*, *12*(16), 5021–5039. https://doi.org/10.5194/bg-12-5021-2015

Letelier, R. M., Bidigare, R. R., Hebel, D. V., Ondrusek, M. E., Winn, C. D., & Karl, D. M. (1993). Temporal variability of phytoplankton community structure based on pigment analysis. *Limnology & Oceanography*, *38*(7), 1420–1437. https://doi.org/10.4319/lo.1993.38.7.1420

Letelier, R. M., Karl, D. M., Abbott, M. R., & Bidigare, R. R. (2004). Light driven seasonal patterns of chlorophyll and nitrate in the lower euphotic zone of the North Pacific Subtropical Gyre. *Limnology & Oceanography*, *49*(2), 508–519. https://doi.org/10.4319/lo.2004.49.2.0508

Lévy, M. (2003). Mesoscale variability of phytoplankton and of new production: Impact of the large-scale nutrient distribution. *Journal of Geophysical Research*, *108*(C11). https://doi.org/10.1029/2002jc001577

Lewis, M. R., Harrison, W. G., Oakey, N. S., Hebert, D., & Platt, T. (1986). Vertical nitrate fluxes in the oligotrophic ocean. *Science*, *234*(4778), 870–873. https://doi.org/10.1126/science.234.4778.870

Liccardo, A., Fierro, A., Iudicone, D., Bouruet-Aubertot, P., & Dubroca, L. (2013). Response of the deep chlorophyll maximum to fluctuations in vertical mixing intensity. *Progress in Oceanography*, *109*, 33–46. https://doi.org/10.1016/j.pocean.2012.09.004

Liu, H., Nolla, H. A., & Campbell, L. (1997). Prochlorococcus growth rate and contribution to primary production in the equatorial and subtropical North Pacific Ocean. *Aquatic Microbial Ecology*, *12*(1), 39–47. https://doi.org/10.3354/ame012039

Llort, J., Langlais, C., Matear, R. J., Moreau, S., Lenton, A., & Strutton, P. G. (2018). Evaluating Southern Ocean carbon eddy-pump from biogeochemical-argo floats. *Journal of Geophysical Research: Oceans*, *123*(2), 971–984. https://doi.org/10.1002/2017jc012861

Loisel, H., & Morel, A. (1998). Light scattering and chlorophyll concentration in case 1 waters: A reexamination. *Limnology & Oceanography*, *43*(5), 847–858. https://doi.org/10.4319/lo.1998.43.5.0847

Longhurst, A., Sathyendranath, S., Platt, T., & Caverhill, C. (1995). An estimate of global primary production in the ocean from satellite radiometer data. *Journal of Plankton Research*, *17*(6), 1245–1271. https://doi.org/10.1093/plankt/17.6.1245

Lutz, V. A., Sathyendranath, S., Head, E. J. H., & Li, W. K. W. (2003). Variability in pigment composition and optical characteristics of phytoplankton in the Labrador Sea and the Central North Atlantic. *Marine Ecology Progress Series*, *260*, 1–18. https://doi.org/10.3354/meps260001

Mann, K. H., & Lazier, J. R. N. (2006). *Dynamics of marine ecosystems: Biological-physical interactions in the oceans* (3rd ed.). Malden, MA, Oxford, UK: Wiley-Blackwell. https://doi.org/10.1002/9781118687901

Maranon, E., Holligan, P. M., Varela, M., Mourin, B., & Bale, A. J. (2000). Highest levels of euphotic layer. *Deep-Sea Research Part I: Oceanographic Research Papers*, *47*, 825–857. https://doi.org/10.1016/s0967-0637(99)00087-4

Martin, J., Coale, K. H., Johnson, K. S., Fitzwater, S. E., Gordon, R. M., Tanner, S. J., et al. (1994). Testing the iron hypothesis in ecosystems of the equatorial Pacific Ocean. *Nature*, *371*(6493), 123–129. https://doi.org/10.1038/371123a0

Martin, J., Tremblay, J. É., Gagnon, J., Tremblay, G., Lapoussière, A., Jose, C., et al. (2010). Prevalence, structure and properties of subsurface chlorophyll maxima in Canadian Arctic waters. *Marine Ecology Progress Series*, *412*, 69–84. https://doi.org/10.3354/meps08666

Marty, J. C., Chiavérini, J., Pizay, M. D., & Avril, B. (2002). Seasonal and interannual dynamics of nutrients and phytoplankton pigments in the western Mediterranean Sea at the DYFAMED time-series station (1991-1999). *Deep-Sea Research Part II: Topical Studies in Oceanography*, *49*(11), 1965–1985. https://doi.org/10.1016/s0967-0645(02)00022-x

McGillicuddy, D. J., & Robinson, A. R. (1997). Eddy-induced nutrient supply and new production in the Sargasso Sea. *Deep-Sea Research Part I: Oceanographic Research Papers*, *44*(8), 1427–1450. https://doi.org/10.1016/s0967-0637(97)00024-1

McGowan, J. A., & Hayward, T. L. (1978). Mixing and oceanic productivity. *Deep-Sea Research*, *25*(9), 771–793. https://doi.org/10.1016/0146-6291(78)90023-1

Mignot, A., Claustre, H., D'Ortenzio, F., Xing, X., Poteau, A., & Ras, J. (2011). From the shape of the vertical profile of in vivo fluorescence to Chlorophyll-a concentration. *Biogeosciences*, *8*(8), 2391–2406. https://doi.org/10.5194/bg-8-2391-2011

Mignot, A., Claustre, H., Uitz, J., Poteau, A., D'Ortenzio, F., & Xing, X. (2014). Understanding the seasonal dynamics of phytoplankton biomass and the deep chlorophyll maximum in oligotrophic environments: A Bio-Argo float investigation. *Global Biogeochemical Cycles*, *28*(8), 856–876. https://doi.org/10.1002/2013gb004781

Millot, C. (1999). Circulation in the Western Mediterranean Sea. *Journal of Marine Systems*, *20*(1–4), 423–442. https://doi.org/10.1016/s0924-7963(98)00078-5

Morel, A. (1988). Optical modeling of the upper ocean in relation to its biogenous matter content (case I waters). *Journal of Geophysical Research*, *93*(C9). 10749. https://doi.org/10.1029/jc093ic09p10749

Morel, A., & Berthon, J.-F. (1989). Surface pigments, algal biomass profiles, and potential production of the euphotic layer: Relationships reinvestigated in view of remote-sensing applications. *Limnology & Oceanography*, *34*(8), 1545–1562. https://doi.org/10.4319/lo.1989.34.8.1545

Morel, A., Claustre, H., & Gentili, B. (2010). The most oligotrophic subtropical zones of the global ocean: Similarities and differences in terms of chlorophyll and yellow substance. *Biogeosciences*, *7*(10), 3139–3151. https://doi.org/10.5194/bg-7-3139-2010

Morel, A., Gentili, B., Claustre, H., Babin, M., Bricaud, A., Ras, J., & Tièche, F. (2007). Optical properties of the "clearest" natural waters. *Limnology & Oceanography*, *52*(1), 217–229. https://doi.org/10.4319/lo.2007.52.1.0217

Morel, A., Huot, Y., Gentili, B., Werdell, P. J., Hooker, S. B., & Franz, B. A. (2007). Examining the consistency of products derived from various ocean color sensors in open ocean (Case 1) waters in the perspective of a multi-sensor approach. *Remote Sensing of Environment*, *111*(1), 69–88. https://doi.org/10.1016/j.rse.2007.03.012

Murty, V. S. N., Gupta, G. V. M., Sarma, V. V., Rao, B. P., Jyothi, D., Shastri, P. N. M., & Supraveena, Y. (2000). Effect of vertical stability and circulation on the depth of the chlorophyll maximum in the Bay of Bengal during May-June, 1996. *Deep-Sea Research Part I: Oceanographic Research Papers*, *47*(5), 859–873. https://doi.org/10.1016/s0967-0637(99)00071-0

Ondrusek, M. E., Bidigare, R. R., Sweet, S. T., Defreitas, D. A., & Brooks, J. M. (1991). Distribution of phytoplankton pigments in the North Pacific Ocean in relation to physical and optical variability. *Deep-Sea Research Part A. Oceanographic Research Papers*, *38*(2), 243–266. https://doi.org/10.1016/0198-0149(91)90082-q

Parslow, J. S., Boyd, P. W., Rintoul, S. R., & Griffiths, F. B. (2001). A persistent subsurface chlorophyll maximum in the Interpolar Frontal Zone south of Australia: Seasonal progression and implications for phytoplankton-light-nutrient interactions. *Journal of Geophysical Research*, *106*(C12), 31543–31557. https://doi.org/10.1029/2000jc000322

Partensky, F., Blanchot, J., Lantoine, F., Neveux, J., & Marie, D. (1996). Vertical structure of picophytoplankton at different trophic sites of the tropical northeastern Atlantic. *Deep-Sea Research Part I: Oceanographic Research Papers*, *43*(8), 1191–1213. https://doi.org/10.1016/0967-0637(96)00056-8

Pérez, F. F., Gilcoto, M., & Rios, A. F. (2003). Large and mesoscale variability of the water masses and the deep chlorophyll maximum in the Azores Front. *Journal of Geophysical Research*, *108*(C7). https://doi.org/10.1029/2000jc000360

Pérez, V., Fernández, E., Marañón, E., Morán, X. A. G., & Zubkov, M. V. (2006). Vertical distribution of phytoplankton biomass, production and growth in the Atlantic subtropical gyres. *Deep-Sea Research Part I: Oceanographic Research Papers*, *53*(10), 1616–1634. https://doi.org/10.1016/j.dsr.2006.07.008

Platt, T., Sathyendranath, S., Caverhill, C. M., & Lewis, M. R. (1988). Ocean primary production and available light: Further algorithms for remote sensing. *Deep-Sea Research Part A. Oceanographic Research Papers*, *35*(6), 855–879. https://doi.org/10.1016/0198-0149(88)90064-7

Poteau, A., Boss, E., & Claustre, H. (2017). Particulate concentration and seasonal dynamics in the mesopelagic ocean based on the backscattering coefficient measured with Biogeochemical-Argo floats. *Geophysical Research Letters*, *44*(13), 6933–6939. https://doi.org/10.1002/2017gl073949

Quéguiner, B. (2001). Biogenic silica production in the Australian sector of the Subantarctic Zone of the Southern Ocean in late summer 1998. *Journal of Geophysical Research*, *106*(C12), 31627–31636. https://doi.org/10.1029/2000jc000249
Ras, J., Claustre, H., & Uitz, J. (2008). Spatial variability of phytoplankton pigment distributions in the Subtropical South Pacific Ocean: Comparison between in situ and predicted data. *Biogeosciences*, *5*(2), 353–369. https://doi.org/10.5194/bg-5-353-2008
Ravichandran, M., Girishkumar, M. S., & Riser, S. (2012). Observed variability of chlorophyll-a using Argo profiling floats in the southeastern Arabian Sea. *Deep-Sea Research Part I: Oceanographic Research Papers*, *65*, 15–25. https://doi.org/10.1016/j.dsr.2012.03.003
Richardson, K., Visser, A. W., & Pedersen, F. B. (2000). Subsurface phytoplankton blooms fuel pelagic production in the North Sea. *Journal of Plankton Research*, *22*(2), 1663–1671. https://doi.org/10.1093/plankt/22.9.1663
Riley, G. A., Stommel, H., & Bumpus, D. F. (1949). Quantitative ecology of the plankton of the western North Atlantic. *Bulletin of the Bingham Oceanographic Collection*, *12*, 1–169. https://ci.nii.ac.jp/naid/10010435137/
Roemmich, D., Alford, M. H., Claustre, H., Johnson, K. S., King, B., Moum, J., et al. (2019). On the future of Argo: A global, full-depth, multi-disciplinary array. *Frontiers in Marine Science*, *6*, 439. https://doi.org/10.3389/fmars.2019.00439
Roesler, C., Uitz, J., Claustre, H., Boss, E., Xing, X., Organelli, E., et al. (2017). Recommendations for obtaining unbiased chlorophyll estimates from in situ chlorophyll fluorometers: A global analysis of WET Labs ECO sensors. *Limnology and Oceanography: Methods*, *15*(6), 572–585. https://doi.org/10.1002/lom3.10185
Sauzède, R., Bittig, H. C., Claustre, H., de Fommervault, O. P., Gattuso, J. P., Legendre, L., & Johnson, K. S. (2017). Estimates of water-column nutrient concentrations and carbonate system parameters in the global ocean: A novel approach based on neural networks. *Frontiers in Marine Science*, *4*, 128. https://doi.org/10.3389/fmars.2017.00128
Scofield, A. E., Watkins, J. M., Osantowski, E., & Rudstam, L. G. (2020). Deep chlorophyll maxima across a trophic state gradient: A case study in the Laurentian Great Lakes. *Limnology and Oceanography*, *65*(10), 2460–2484. https://doi.org/10.1002/lno.11464
Sharples, J., Moore, C. M., Rippeth, T. P., Holligan, P. M., Hydes, D. J., Fisher, N. R., & Simpson, J. H. (2001). Phytoplankton distribution and survival in the thermocline. *Limnology & Oceanography*, *46*(3), 486–496. https://doi.org/10.4319/lo.2001.46.3.0486
Sharples, J., & Tett, P. (1994). Modeling the effect of physical variability on the midwater chlorophyll maximum. *Journal of Marine Research*, *52*(2), 219–238. https://doi.org/10.1357/0022240943077109
Silsbe, G. M., & Malkin, S. Y. (2016). Where light and nutrients collide: The global distribution and activity of subsurface chlorophyll maximum layers. In *Aquatic microbial ecology and biogeochemistry: A Dual perspective* (pp. 1–300). https://doi.org/10.1007/978-3-319-30259-1_12
Steele, J. H. (1964). A study of the production in the Gulf of Mexico. *Journal of Marine Research*, *22*, 211–222.
Steele, J. H., & Yentsch, C. S. (1960). The vertical distribution of chlorophyll. *Journal of the Marine Biological Association of the United Kingdom*, *39*(2), 217–226. https://doi.org/10.1017/s0025315400013266
Stramski, D., Reynolds, R. A., Kahru, M., & Mitchell, B. G. (1999). Estimation of particulate organic carbon in the ocean from satellite remote sensing. *Science*, *285*(5425), 239–242. https://doi.org/10.21236/ada629587
Sugimoto, T., Tadokoro, K., & Furushima, Y. (1995). Climate and weather effects on the chlorophyll concentration in the northwestern North Pacific. In H. In Sakai, & Y. Nozaki (Eds.), *Biogeochemical processes and ocean flux in the western pacific* (pp. 575–592). Terra Scientific Publishing Co.
Takahashi, M., & Hori, T. (1984). Abundance of picophytoplankton in the subsurface chlorophyll maximum layer in subtropical and tropical waters. *Marine Biology*, *79*(2), 177–186. https://doi.org/10.1007/bf00951826
Taylor, A. H., Geider, R. J., & Gilbert, F. J. H. (1997). Seasonal and latitudinal dependencies of phytoplankton carbon-to-chlorophyll a ratios: Results of a modeling study. *Marine Ecology Progress Series*, *152*(1–3), 51–66. https://doi.org/10.3354/meps152051
Taylor, A. H., Harris, J. W., & Aiken, J. (1986). The interaction of physical and biological processes in a model of the vertical distribution of phytoplankton under stratification. In *Marine interfaces ecohydrodynamics* (pp. 313–330).
Thushara, V., Vinayachandran, P. N. M., Matthews, A. J., Webber, B. G. M., & Queste, B. Y. (2019). Vertical distribution of chlorophyll in dynamically distinct regions of the southern Bay of Bengal. *Biogeosciences*, *16*(7), 1447–1468. https://doi.org/10.5194/bg-16-1447-2019
Tripathy, S. C., Pavithran, S., Sabu, P., Pillai, H. U. K., Dessai, D. R. G., & Anilkumar, N. (2015). Deep chlorophyll maximum and primary productivity in Indian Ocean sector of the Southern Ocean: Case study in the Subtropical and Polar Front during austral summer 2011. *Deep-Sea Research Part II: Topical Studies in Oceanography*, *118*, 240–249. https://doi.org/10.1016/j.dsr2.2015.01.004
Uitz, J., Claustre, H., Morel, A., & Hooker, S. B. (2006). Vertical distribution of phytoplankton communities in open ocean: An assessment based on surface chlorophyll. *Journal of Geophysical Research*, *111*(8). https://doi.org/10.1029/2005jc003207
Vaillancourt, R. D., Marra, J., Seki, M. P., Parsons, M. L., & Bidigare, R. R. (2003). Impact of a cyclonic eddy on phytoplankton community structure and photosynthetic competency in the subtropical North Pacific Ocean. *Deep-Sea Research Part I: Oceanographic Research Papers*, *50*, 829–847. https://doi.org/10.1016/s0967-0637(03)00059-1
Varela, R. A., Cruzado, A., & Tintoré, J. (1994). A simulation analysis of various biological and physical factors influencing the deep-chlorophyll maximum structure in oligotrophic areas. *Journal of Marine Systems*, *5*(2), 143–157. https://doi.org/10.1016/0924-7963(94)90028-0
Varela, R. A., Cruzado, A., Tintore, J., & Garcia Ladona, E. (1992). Modeling the deep-chlorophyll maximum: A coupled physical- biological approach. *Journal of Marine Research*, *50*(3), 441–463. https://doi.org/10.1357/002224092784797638
Venrick, E. L., McGowan, J. A., & Mantyla, A. W. (1973). Deep maxima of photosynthetic chlorophyll in the Pacific Ocean. *Fishery Bulletin US*, *71*, 41–52.
Vinogradov, M. E. (1981). Ecosystems of equatorial upwellings. In A. R. Longhurst (Ed.), *Analysis of marine ecosystems* (pp. 69–93). Academic Press.
Voituriez, B., & Herbland, A. (1979). The use of the salinity maximum of the equatorial undercurrent for estimating nutrient enrichment and primary production in the Gulf of Guinea. *Deep-Sea Research Part A. Oceanographic Research Papers*, *26*(1), 77–83. https://doi.org/10.1016/0198-0149(79)90087-6
Waite, A. M., & Nodder, S. D. (2001). The effect of in situ iron addition on the sinking rates and export flux of Southern Ocean diatoms. *Deep-Sea Research Part II: Topical Studies in Oceanography*, *48*(11–12), 2635–2654. https://doi.org/10.1016/s0967-0645(01)00012-1
Westberry, T., Behrenfeld, M. J., Siegel, D. A., & Boss, E. (2008). Carbon-based primary productivity modeling with vertically resolved photoacclimation. *Global Biogeochemical Cycles*, *22*(2). https://doi.org/10.1029/2007gb003078
Westwood, K. J., Griffiths, F. B., Webb, J. P., & Wright, S. W. (2011). Primary production in the Sub-Antarctic and Polar Frontal Zones south of Tasmania, Australia; SAZ-Sense survey. *Deep-Sea Research Part II: Topical Studies in Oceanography*, *58*(21–22), 2162–2178. https://doi.org/10.1016/j.dsr2.2011.05.017
Winn, C. D., Campbell, L., Christian, J. R., Letelier, R. M., Hebel, D. V., Dore, J. E., et al. (1995). Seasonal variability in the phytoplankton community of the North Pacific Subtropical Gyre. *Global Biogeochemical Cycles*, *9*(4), 605–620. https://doi.org/10.1029/95gb02149
Wong, A., Keeley, R., & Carval, T., & theArgoDataManagement Team. (2020). *Argo quality control manual technical report, ArgoData Management team*.

Wright, S. W., & Van den Enden, R. L. (2000). Phytoplankton community structure and stocks in the East Antarctic marginal ice zone (BROKE survey, January-March 1996) determined by CHEMTAX analysis of HPLC pigment signatures. *Deep-Sea Research Part II: Topical Studies in Oceanography*, *47*(12–13), 2363–2400. https://doi.org/10.1016/s0967-0645(00)00029-1

Wroblewski, J. S. (1989). A model of the spring bloom in the North Atlantic and its impact on ocean optics. *Limnology & Oceanography*, *34*(8), 1563–1571. https://doi.org/10.4319/lo.1989.34.8.1563

Xing, X., Briggs, N., Boss, E., & Claustre, H. (2018). Improved correction for non-photochemical quenching of in situ chlorophyll fluorescence based on a synchronous irradiance profile. *Optics Express*, *26*(19), 24734. https://doi.org/10.1364/oe.26.024734

Yool, A., & Tyrrell, T. (2003). Role of diatoms in regulating the ocean's silicon cycle. *Global Biogeochemical Cycles*, *17*(4). https://doi.org/10.1029/2002gb002018

Zhang, Y., Jiao, N., & Hong, N. (2008). Comparative study of picoplankton biomass and community structure in different provinces from subarctic to subtropical oceans. *Deep-Sea Research Part II: Topical Studies in Oceanography*, *55*(14–15), 1605–1614. https://doi.org/10.1016/j.dsr2.2008.04.014